Earth Science Informatics
https://doi.org/10.1007/s12145-024-01403-6

RESEARCH

Estimating S-wave amplitude for earthquake early warning in New Zealand: Leveraging the first 3 seconds of P-Wave

Chanthujan Chandrakumar[1] · **Marion Lara Tan**[1] · **Caroline Holden**[2] · **Max Stephens**[3] · **Amal Punchihewa**[4] · **Raj Prasanna**[1]

Received: 25 May 2024 / Accepted: 29 June 2024

Abstract
This study addresses the critical question of predicting the amplitude of S-waves during earthquakes in Aotearoa New Zealand (NZ), a highly earthquake-prone region, for implementing an Earthquake Early Warning System (EEWS). This research uses ground motion parameters from a comprehensive dataset comprising historical earthquakes in the Canterbury region of NZ. It explores the potential to estimate the damaging S-wave amplitude before it arrives, primarily focusing on the initial P-wave signals. The study establishes nine linear regression relationships between P-wave and S-wave amplitudes, employing three parameters: peak ground acceleration, peak ground velocity, and peak ground displacement. Each relationship's performance is evaluated through correlation coefficient (R), coefficient of determination (R^2), root mean square error (RMSE), and 5-fold Cross-validation RMSE, aiming to identify the most predictive empirical model for the Canterbury context. Results using a weighted scoring approach indicate that the relationship involving P-wave Peak Ground Velocity (Pv) within a 3-second window strongly correlates with S-wave Peak Ground Acceleration (PGA), highlighting its potential for EEWS. The selected empirical relationship is subsequently applied to establish a P-wave amplitude (Pv) threshold for the Canterbury region as a case study from which an EEWS could benefit. The study also suggests future research exploring complex machine learning models for predicting S-wave amplitude and expanding the analysis with more datasets from different regions of NZ.

Keywords Earthquake early warning · Low-cost seismometers · The PLUM · MEMS · Warning systems · S-wave estimation · Earthquake resilience · Earthquake detection

Introduction

Earthquakes pose a significant hazard in Aotearoa New Zealand (NZ), one of the most seismically active regions globally (Anderson and Webb 1994). Annually, over a hundred earthquakes of magnitude four or higher are recorded (GeoNet 2023). The devastating impacts of significant seismic events, such as the 2010/2011 Canterbury sequence and the 2016 Kaikōura earthquake, underscore the urgent need for effective mitigation strategies (Potter et al. 2015); Stevenson et al. (2011, 2017). Earthquake Early Warning System (EEWS) emerges as a vital technology to reduce earthquake-related damages by providing advance alerts, yet NZ lacks an official national EEWS (Becker et al. 2020). The GeoNet program, while serving as the official source of seismic information, does not provide early warnings (GeoNet 2017; GNS Science 2023). The absence of a formal EEWS is primarily attributed to the high costs associated with developing and maintaining such advanced systems, presenting a substantial challenge for their implementation in NZ (Brooks et al. 2021; Prasanna et al. 2022).

The increasing global interest in cost-effective EEWSs has led to the adoption of low-cost micro-electromechanical systems (MEMS)-based sensors. Since their introduction in the early 1990s (Holland 2003), these sensors have been effectively utilised in seismic applications for real-time

Communicated by: Hassan Babaie

✉ Chanthujan Chandrakumar
c.chandrakumar2@massey.ac.nz

[1] Joint Centre for Disaster Research, Massey University, Wellington, New Zealand

[2] SeismoCity Ltd, Wellington, New Zealand

[3] Faculty of Engineering, Civil and Environmental Engineering, University of Auckland, Auckland, New Zealand

[4] ADP Consultancy, Palmerston North, New Zealand

public alerting across various regions, including Taiwan (Wu et al. 2013), China (Peng et al. 2019), California (Clayton et al. 2015), and Costa Rica (Brooks et al. 2021), albeit mostly in experimental setups. In NZ, the CRISiSLab team at Massey University has developed an experimental, community-engaged EEWS utilising Raspberry Shake 4D seismographs equipped with MEMS-based accelerometers (Prasanna et al. 2022). The system employs the Propagation of the Local Undamped Motion (PLUM) algorithm, known for its robustness and straightforward approach to detecting seismic activities and issuing alerts without the need to estimate detailed seismic event characteristics (Chandrakumar et al. 2023).

A significant limitation of the PLUM algorithm is its maximum warning time of 10 s, primarily due to its reliance solely on S-wave detection. This study proposes addressing this limitation by leveraging the earlier arrival of P-waves (Kodera 2018). A suitable P-wave detection algorithm has already been identified in a previous study (Chandrakumar et al. 2023), paving the way for this advancement. The system can capitalise on P-wave detection to extend warning times within the PLUM framework by establishing a reliable empirical relationship between P-wave and S-wave amplitudes (Kodera 2018). This relationship offers two significant advantages. First, it enhances the effectiveness of the PLUM algorithm by providing more lead time for preparedness. Second, it enables the determination of P-wave thresholds for the early detection of significant shaking.

In this context, this research addresses a critical gap in NZ's EEWS capabilities by establishing robust empirical relationships between P-wave and S-wave amplitude parameters specific to the country's unique seismic landscape using linear regression models. Subsequently, the study identifies the most suitable empirical relationship for application in NZ's highly seismic Canterbury region. A case study utilising the chosen relationship is presented to define effective EEW alert thresholds for P-waves in the Canterbury region, demonstrating a practical application of the research findings.

The structure of this article is organised as follows: The second section offers a brief overview of the literature on P-wave to S-wave amplitude relationships from studies conducted globally. The third section details the methodology employed in this research. The fourth section presents the comprehensive results, which are then discussed in the fifth section in the context of the established empirical relationships. Building on these results, the sixth section introduces a case study that applies the selected empirical relationship to determine thresholds for felt earthquakes in NZ. Finally, the seventh section provides a conclusive summary and key takeaways, highlighting the significance of this research.

Background on P-wave and S-wave amplitude relationships

Researchers worldwide have explored various methods utilising P-wave measurements to estimate ground shaking, either by determining earthquake magnitude or predicting the amplitude of S-waves. One notable approach originated in Japan during the 1990s with the UrEDAS system, which pioneered the use of P-wave arrival to estimate earthquake magnitude and location (Nakamura 2004). Following this, Allen and Kanamori (2003) introduced a method that estimates earthquake magnitude from the frequency content of P-wave arrivals.

In the Japanese seismic landscape, Yamamoto et al. (2008) introduced a new intensity parameter called M_I, showcasing that, for Japanese seismic data, P-wave intensity is consistently lower than S-wave intensity by approximately an M_I value of 1. Meanwhile, in Taiwan, researchers conducted a comprehensive analysis of the relationship between P-wave and S-wave amplitude. They used various measurements from P and S waves, including Peak Ground Acceleration (Pa), Peak Ground Velocity (Pv), Peak Ground Displacement (Pd) and Period parameter (τ_C) from the 3 s following the P-wave detection, as well as Peak Ground Velocity (PGV) and Peak Ground Displacement (PGD) of S-waves for 26 damaging earthquakes (Wu and Kanamori 2005a, b). Out of these parameters, they were able to select the most suitable relationship for their system, ultimately establishing Pd and τ_C thresholds for EEW. Further work investigated the relationship between Pd and PGV using records from Japan, Taiwan, and southern California (Wu and Kanamori 2008; Wu and Mittal 2021).

Researchers from USA, China and Italy contributed to advancing approaches by utilising Pd (measured within 3 s after P-wave detection) as a proxy for predicting PGV (Böse et al. 2009a; Caruso et al. 2017; Wang et al. 2020; Zollo et al. 2014). In contrast, Colombelli et al. (2015) established an empirical relationship between three peak amplitude parameters of the P-wave window (Pa, Pv and Pd) and PGV.

While some studies suggest that predicting the ground shaking of an earthquake using just a few seconds of initial P-wave data is achievable (Olson and Allen 2005; Zollo et al. 2006), others indicate that the estimation of ground shaking tends to saturate for larger events with longer rupture durations (Hoshiba et al. 2011; Rydelek and Horiuchi 2006). Predicting the ground shaking of significant seismic events with limited real-time seismic data has become increasingly challenging due to the complexities involved. Larger crustal earthquakes with magnitudes (M) of 6, 7, and 8 are associated with fault lengths of about 10 km, 30 km, and 100 km, respectively, with rupture velocities close to of

3 km/s. Consequently, assuming a unilateral rupture, it could take up to 3, 10, and 30 s to rupture these faults completely (Wells and Coppersmith 1994; Yamamoto et al. 2008). Also, it has become quite challenging to determine the ground shakings of significant seismic events with limited real-time seismic data (Yamamoto et al. 2008). However, it is essential to note that these methods are still valuable for estimating lower bounds of expected ground shakings, aiding in the early assessment of earthquake strength (Kanamori 2005).

These studies on P-wave and S-wave relationships worldwide have contributed significantly to improving EEW research. However, most of these findings are predominantly rooted in research outside NZ's unique geological and tectonic context. Therefore, researching and constructing a relationship between P and S-wave amplitude is crucial to successfully developing an EEWS tailored to NZ's unique geological and tectonic conditions. Findings in NZ also adds to the discourse in global research.

Method

Data collection

The data for this study are strategically sourced from the Canterbury Region, NZ, chosen for its history of significant seismic activity and the notable impact of past earthquakes (Stevenson et al. 2011, 2017). This research utilises the Canterbury Network (CanNet), a low-cost strong motion network established by GeoNet before the 2010–2011 Canterbury earthquake sequence. CanNet is equipped with MEMS-based accelerometers designed to effectively record ground motions (Avery et al. 2004; Berrill et al. 2011). The selection of CanNet is deliberate, as its accelerometers closely match the response characteristics of the sensors used in the CRISiSLab EEWS. This ensures that the seismic data collected are reliable and relevant from a network mirroring the CRISiSLab EEWS.

The timeframe from 2010 to 2023 is chosen for data collection because it corresponds to the period during which GeoNet actively catalogued and recorded P-wave and S-wave picks for most of the CanNet recordings. This pre-existing identification of arrival times is critical. It significantly reduces the need for manual pickings across the numerous earthquake ground motion recordings.

The dataset compiled from this collection phase comprises 5254 earthquake waveforms captured from MEMS-based accelerometers, corresponding to 3245 earthquakes with a magnitude exceeding 3 ($M > 3$). Even though the data are limited, they serve the need to make a baseline for implementing a relationship between P and S-waves as an initial foundation. This focused dataset provides a strong foundation for investigating these relationships and advancing the operational capabilities of low-cost EEWSs.

Data analysis

Data inspection and selection

The initial phase of the research involves an assessment of data quality to ensure the reliability of subsequent analyses. Each waveform from the 5254 records in the dataset is visually inspected during this phase. A specialised tool is developed to facilitate this inspection that allows for the individual review of waveforms (Fig. 1). This tool generates four plots for each record, each serving a specific role in the inspection process. The first plot displays the vertical acceleration record, highlighting P and S-wave picks reported by GeoNet with distinctive red and blue vertical lines, facilitating precise waveform analysis (Fig. 1a). For a closer examination, the second plot provides an enlarged view of the absolute vertical acceleration record, focusing on a 5-second window around the P-wave pick to inspect the P-wave arrival (Fig. 1b). The third and fourth plots showcase horizontal acceleration records in the HNE: east component and HNN: north component directions, with the S-wave pick marked by a blue vertical line (Fig. 1c and d).

During this phase, the focus is on verifying the accuracy of the P and S-wave picks recorded by GeoNet. Records with accurately identified picks are selected for further analysis, while those with erroneous picks are excluded. This process resulted in 4330 valid waveforms. Subsequently, these recordings are classified according to Site Classes defined for NZ based on soil characteristics (Dobry et al. 2000). The majority of the data belonged to Site Class D, and to maintain consistency in soil characteristics, only records from this class are retained, refined dataset of 3542 waveforms.

To ensure the relevancy and suitability of the data for the study, ground motion records are exclusively retained from stations situated within a 30-kilometre epicentral distance from each earthquake event, a selection criterion supported by previous research (Böse et al. 2009; Tsuno 2021; Zollo et al. 2010). Two key considerations drove this strategy. First, it guarantees data relevancy, as P and S waves are less likely to be contaminated by other waves in the coda. Proximity to the epicentre enables the accurate detection of both P and S-waves. Second, data quality is enhanced closer to the epicentre due to a reduced noise-to-signal ratio, improving the precision of empirical relationships.

Additionally, a condition is imposed to include a maximum of four station records for each earthquake event. This filtering process results in the final selection of 763 earthquake events, with magnitudes ranging from 3 to 6.6, yielding 1,251 earthquake ground motion records suitable for further analysis. Figure 2 illustrates the Canterbury region chosen for this study, highlighting the seismic

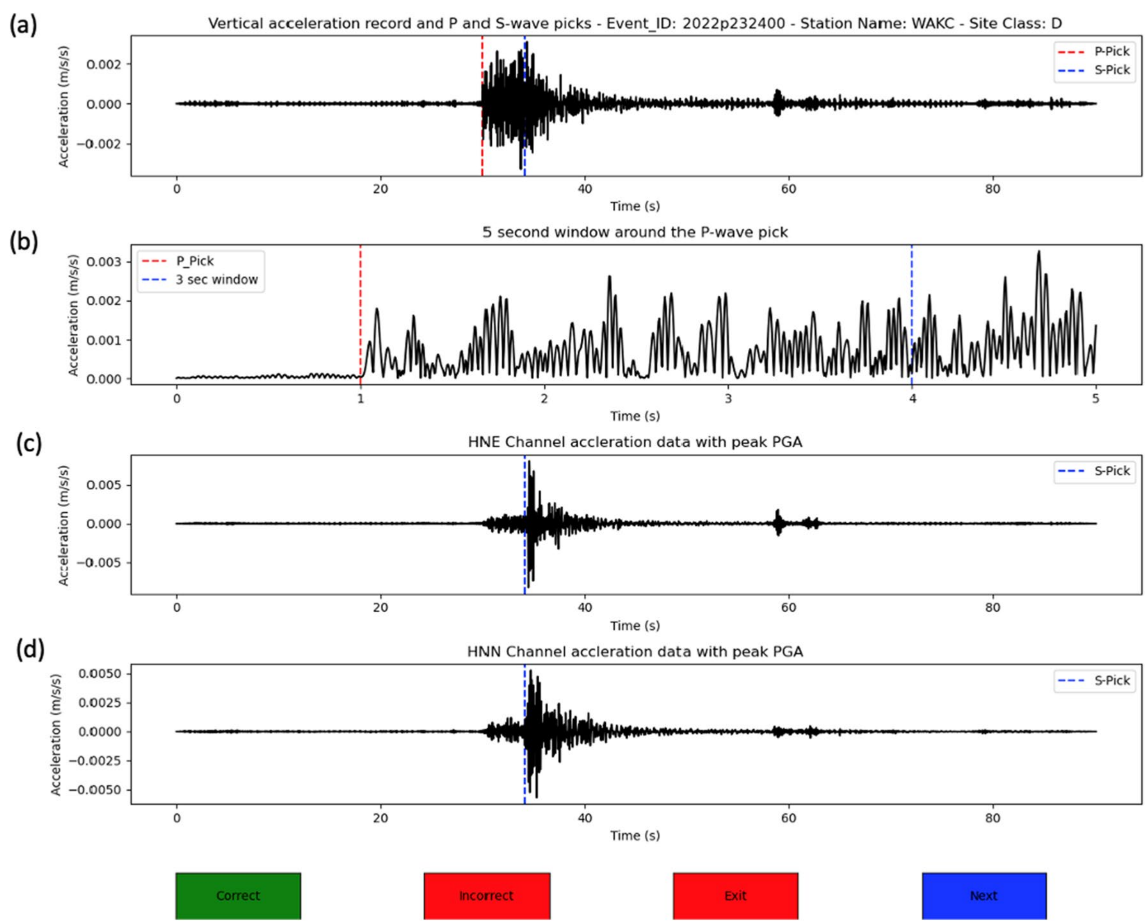

Fig. 1 Interface of a seismic waveform inspection tool. **a** shows a vertical acceleration record with P and S-wave picks marked by red and blue lines, respectively. **b** displays an enlarged view of the absolute vertical record around the P-wave pick for detailed analysis. Panels (**c**) and (**d**) present horizontal acceleration records in the east (HNE) and north (HNN) directions, with S-wave picks indicated by blue lines

station locations and the epicentral locations of the earthquakes. Further, Table 1 summarises the earthquake magnitudes and the corresponding number of events.

Data allocation for model training and evaluation

After filtering, the dataset is subjected to time-based splitting, where training and testing sets are selected based on their temporal order (Lyu et al. 2021). Time-based splitting ensures the model is trained on historical data and evaluated on new, unseen data. This allocation strategy facilitates comprehensive model development and ensures a reliable evaluation using independent data.

I. Training Dataset: It consists of 1021 ground motion recordings of the filtered data from 2010 to 2019, which are used to develop the model.

II. Testing Dataset: It contains 230 recordings of the filtered data from 2020 to 2023, which are reserved for model evaluation.

Parameters used for analysis

The analytical focus of the study centred on two distinct time windows: the three-second interval immediately following the P-wave pick and the subsequent time window corresponding to the arrival of the S-wave. The selection of a 3-second time window for the P-wave phase draws from literature, emphasising the effectiveness of this choice (Wu and Kanamori 2005a). It balances achieving accurate S-wave amplitude estimation and providing a sufficiently wide warning window with reduced blind zone for an EEWS (Böse et al. 2009a; Caruso et al. 2017; Wang et al. 2020; Y.-M. Wu and Mittal 2021).

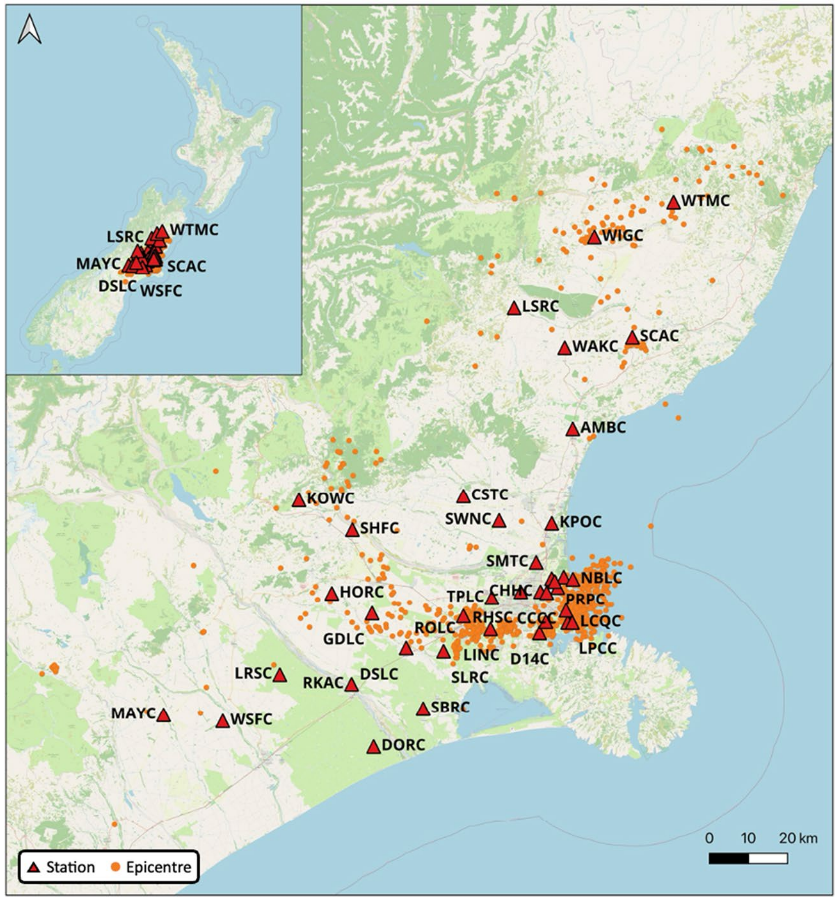

Fig. 2 Map of the Canterbury region in NZ, showing the locations of seismic stations and the epicentres of selected earthquake events used in this study

Standard metrics such as Peak Ground Acceleration, Peak Ground Velocity, and Peak Ground Displacement can be used to represent the amplitude of seismic waves for an earthquake (Y. M. Wu and Zhao 2006; Y.-M. Wu and Kanamori 2008). Therefore, this study computed six seismic parameters to establish relationships between P and S-wave amplitude.

For the selected P-wave window, calculations for estimating the amplitude of the P-wave include the Peak Ground Acceleration (Pa), the Peak Ground Velocity (Pv), and the Peak Ground Displacement (Pd) of the P-wave. These calculations are based on the vertical acceleration, velocity, and displacement records, as P-waves predominantly exhibit motion in the vertical direction (Y.-M. Wu 2019; Zhang et al. 2003).

Subsequently, for the S-wave window, key parameters to estimate the amplitude of S-waves: the Peak Ground Acceleration (PGA), the Peak Ground Velocity (PGV), and the Peak Ground Displacement (PGD) are calculated. Data from the HNE (east-west direction) and HNN (north-south direction) channels are utilised to capture these peak values, given that S-waves predominantly exhibit motion in the horizontal direction (Shearer 2009). The PGA, PGV, and PGD values are calculated using the RotD50 method for the S-waves (Boore, 2010).

Before calculating the P-wave and S-wave parameters, the chosen ground motion recordings are filtered using a Butterworth-Bandpass filter from 0.1 to 20 Hz. This filtering step retains the earthquake signal's frequency content of interest and removes low-frequency and high-frequency ambient noise (Claerbout 1964; Virtanen et al. 2020).

Table 2 summarise the parameters used in this study and their respective abbreviations.

It is important to note that this study does not focus on determining the τ_C for the P-wave window, as observed in various studies that seek to establish a relationship between

Table 1 Overview of earthquake magnitudes and event counts in the dataset

Magnitude (M) range	Number of events
3 to 4	596
4 to 5	150
5 and above	17
Total	763

Table 2 Abbreviations and descriptions of the parameters used for analysis

Abbreviation	Description
Pa	Peak Ground Acceleration calculated for the P-wave window
Pv	Peak Ground Velocity calculated for the P-wave window
Pd	Peak Ground Displacement calculated for the P-wave window
PGA	Peak Ground Acceleration calculated for the S-wave window
PGV	Peak Ground Velocity calculated for the S-wave window
PGD	Peak Ground Displacement calculated for the S-wave window

τ_C and earthquake magnitude (M) (Wang et al. 2020; Wu and Kanamori 2005a, b). Instead, the primary focus is exploring relationships between P and S-wave amplitudes.

Outlier test

Before choosing the model, it is crucial to systematically identify and remove outliers from the dataset to ensure the robustness and accuracy of the models. Outliers, which can significantly skew results, are detected using the Interquartile Range (IQR) method (Taylor 2018; Gianluca Malato 2021). The outlier method works as follows,

1. Calculate the dataset's first quartile (Q1) and third quartile (Q3). The first quartile is the value at the 25th percentile, and the third is at the 75th percentile.
2. Compute the IQR as the difference between Q3 and Q1 (IQR = Q3 - Q1). The IQR represents the range of the middle 50% of the data.
3. Define the lower and upper outlier thresholds using the following formulas:

   a Lower threshold = Q1–1.5 * IQR
   b Upper threshold = Q3 + 1.5 * IQR

4. Identify any data points that fall below the lower threshold or above the upper threshold. These observations are considered outliers.

This statistical approach is applied separately to the training and testing datasets to ensure the integrity of the model evaluation. This separation is critical to prevent data leakage, which could lead to overly optimistic performance estimates and compromise the model's generalisability. The outlier removal process affected approximately 0.4–0.5% of the training and testing datasets across all relationships. Further, Figs. 7, 8, 9, 10, 11 to 12 in the Appendix illustrate the data before and after removing outliers for training and testing datasets across the nine relationships intended for construction.

Linear regression analysis

Linear regression is a straightforward approach used in seismology to estimate S-wave amplitudes using P-wave data. Its simplicity and ease of implementation make it an ideal choice for smaller datasets, allowing for the establishment of a reliable baseline relationship between P-wave and S-wave amplitudes. This method has been substantiated by several studies in the literature, which have demonstrated its effectiveness in accurately modelling relationships within the seismic data context (Y.-M. Wu and Mittal 2021; Yamamoto et al. 2008).

Several strategic considerations drove this study's use of a linear regression model. While machine learning models are increasingly popular due to their ability to handle complex datasets and provide accurate predictions, their application in seismology presents unique challenges (Abdalzaher et al. 2023; Hsu and Huang 2021; Zhu et al. 2022). Complex models, such as Convolutional Neural Networks (CNNs) or Recurrent Neural Networks (RNNs), require large datasets to effectively learn and generalise without overfitting (Jon Reilly 2024; Pragati Baheti 2021). Given the specific context of our study, where the dataset comprised MEMS-based ground motion data with a relatively limited size, there is a significant risk that a more complex model could yield unreliable predictions. This concern guided the choice towards using a simple linear regression model.

The computed parameters from the P-wave and S-wave windows served as the basis for establishing nine distinct linear regression relationships between P-wave and S-wave characteristics. To enhance the interpretability and robustness of these relationships, raw parameter values are transformed into logarithmic (log10) base values. This transformation significantly reduces the influence of extreme outliers and stabilises variance, making the data more suitable for linear modelling. Additionally, converting to logarithmic scales compresses the data range, simplifying the analysis and facilitating a more linear representation of the data. This method aids in establishing meaningful correlations and enhances the overall reliability and robustness of the empirical relationships.

The chosen linear regression equation takes the form of **y = ax + b**, where x represents the independent variable (in our study, the amplitude of the P-waves, denoted as Pa, Pv, or Pd) and 'y' represents the dependent variable (the amplitude of the S-waves, represented as PGA, PGV, or PGD). The values for 'a' and 'b' in this equation are determined using the least squares method to find the best-fit linear relationship between the P-wave and S-wave amplitudes. Specifically, 'a' represents the slope of the regression line, indicating the rate of change in the S-wave amplitude concerning changes in the P-wave amplitude, while 'b' represents the intercept, denoting the estimated S-wave amplitude when the P-wave amplitude is zero (Barbur et al. 1994; Draper and Smith 2014).

Following the construction of the linear regression models, the residuals of each model were subjected to an error distribution analysis to evaluate the S-wave amplitude estimation. This included calculating the mean error, median error, standard deviation, and mean absolute error (MAE) for the residuals.

Evaluating the generalisability and suitability of empirical relationships

A set of metrics derived from the established linear regression models are used to evaluate generalisability and select the study's optimal empirical relationship. Further, a weighted scoring approach is employed to quantify the efficacy of each of the nine models.

Metrics

a The correlation coefficient (R)

It measures the strength and direction of a linear relationship between two variables on a scatter plot (Draper and Smith 2014). For linear regression involving two variables x (P-wave amplitude parameter) and y (S-wave amplitude parameter), R ranges from − 1 to 1. A value of 1 indicates a perfect positive linear relationship, where increases in $x$correspond to increases in y. Conversely, a value of -1 denotes a perfect negative linear relationship, where increases in x correspond to decreases in y. A value of 0 signifies no linear correlation between the variables. R is given by the formula:

$$R = \frac{\sum_i^n \sum \left(x_i - \bar{x}\right)\left(y_i - \bar{y}\right)}{\sqrt{\sum_i^n \sum \left(x_i - \bar{x}\right)^2 \sum_i^n \sum \left(y_i - \bar{y}\right)^2}} \tag{1}$$

where x_i and y_i are amplitude parameter values, and $\bar{x}$ and $\bar{y}$ are the mean values of the amplitude parameters for the P and S-waves, respectively.

b The coefficient of determination (R²)

It represents the proportion of the variance in the dependent variable that is predictable from the independent variables. It ranges from 0 to 1 where an R^2 value of 1 indicates that the regression predictions perfectly fit the data, and 0 suggests that the model does not explain any variability in the response data around its mean. The R^2 is the square value of R.

iii. The Root Mean Square Error (RMSE)

It measures the standard deviation of residuals or prediction errors, providing insights into how much deviation occurs from the observed data points to the predictions made by the regression model. This is crucial for assessing a model's accuracy, with lower RMSE values indicating a better fit to the data. RMSE is given by the formula,

$$\text{RMSE} = \sqrt{\frac{\sum_i^n \sum \left(y_i - \hat{y}_i\right)^2}{n}} \tag{2}$$

where y_i is the observed amplitude value, $\hat{y}_i$ is the predicted amplitude value for the S-wave using the linear regression model, and n is the number of observations used.

iv. 5-fold Cross Validation RMSE

It is a statistical method employed to ensure the generalisability of a constructed model. This research utilised a K-fold Cross-validation approach with K equal to 5, chosen to achieve a good balance between the model construction and validation. The training dataset (2010 to 2019) is partitioned into five equal segments. Four segments are used to train the model for each validation cycle, and the remaining segment serves as the test set. This process iterates until each fold has been used for validation exactly once. In this investigation, for each empirical relationship, the RMSE is computed across five distinct folds within the training dataset. RMSE quantifies the average magnitude of the prediction error. By assessing RMSE across all folds, the study can discern how consistently the model performs. Cross-validation is conducted on the training dataset to avoid data leakage and ensure the integrity of performance evaluations. The test dataset is reserved for the final assessment of the model, thereby preventing any bias in the model's estimated ability to generalise and ensuring an unbiased evaluation on new, unseen data.

Method for selecting the most suitable Linear Regression Relationship.

a Evaluation with Testing Data

The models developed are evaluated using an independent test dataset from 2020 to 2023. This phase critically assesses each model's performance on new, unseen data, essential for verifying their robustness. The effectiveness and generalisability of the models are determined by comparing the R^2 and RMSE values from this test dataset against those from the training phase. This approach ensures that the models perform well on historical data and are reliable and accurate when applied to predict future seismic events.

b Overfitting and Underfitting Assessment

Assessing overfitting and underfitting is crucial for ensuring the robustness of constructed models, as these phenomena can significantly affect a model's predictive accuracy on new data. Overfitting occurs when a model is overly tailored to the training data and performs well on this data but poorly generalises to new datasets (Tigran 2022; Will Koehrsen 2018). This often results in models that are tailored too closely to the specifics of the training data. In contrast, underfitting happens when models are too simplistic, failing to capture essential relationships within the data, leading to suboptimal performance on training and testing datasets (Tigran 2022; Will Koehrsen 2018).

The nature of overfitting and underfitting within each constructed linear regression model is analysed using the previously introduced metrics: R^2 and RMSE for both training and testing datasets and RMSE values derived from 5-fold Cross-validation of the training data.

iii. Weighted Scoring Approach

A weighted scoring framework is implemented to aggregate multiple performance metrics into a unified measure of model efficacy, which facilitates the identification of the most appropriate linear regression relationship (Griffith and Headley 1997; Nicholas Morpus 2024). The performance metrics considered are R^2 for the training dataset (Trained R^2), RMSE for the training dataset (Trained RMSE), the mean RMSE from 5-fold Cross-validation (Mean of 5-fold Cross-validation RMSE), R^2 for the testing dataset (Tested R^2), and RMSE for the testing dataset (Tested RMSE). These metrics are normalised to ensure comparability; higher values of R^2 are indicative of better performance, while lower values of RMSE represented lower error rates.

The following factors outline the assigned weights to various evaluation metrics employed in the model selection process and their rationale behind the chosen values.

The Mean of 5-fold Cross-validation RMSE is given the highest weight (0.6) to select the most suitable relationship. This metric is crucial for accurately estimating the model's performance across diverse data subsets; prioritising a lower mean of 5-fold Cross-validation RMSE ensures that the chosen model can generalise effectively and remain reliable in real-world scenarios with potentially varying data characteristics.

Tested RMSE, weighted at 0.3, is the next most important factor. This metric directly assesses the model's performance on entirely new data, a crucial factor for the practical deployment of an EEWS. In an EEWS, encountering unseen data is the norm, emphasising the need for a model that can reliably predict earthquakes under such conditions.

Trained RMSE receives a weight of 0.2, signifying its role in indicating the model's efficacy in capturing and learning from historical data. While a lower Trained RMSE is desirable, it holds less weight than the model's generalisability and performance on unseen data.

Tested R^2 and Trained R^2 are assigned a weight of 0.1 each. While R^2 can be a valuable tool for initial exploration and assessing fit quality in linear models, it is ultimately de-emphasised in favour of RMSE for final model selection. Two factors drive this decision: RMSE possesses a clear unit (error in the original units), facilitating a more straightforward interpretation of the model's performance. Additionally, RMSE exhibits less susceptibility to overfitting compared to R^2. Table 3 displays the weights assigned to the chosen metrics.

The formula for calculating the weighted score of each model integrates these normalised metrics and their respective weights to derive a composite measure of performance is expressed as:

$$\begin{aligned}\text{Weighted Score} = [& (\textit{Normalised Trained } R^2 \times 0.1) \\ & + (\textit{Normalised Tested} R^2 \times 0.1) \\ & + (\text{Normalised Trained RMSE} \times 0.2) \\ & + (\text{Normalised Tested RMSE} \times 0.3) \\ & + (\text{Normalised Cross} - \text{Validation RMSE} \times 0.6)]\end{aligned} \tag{3}$$

Results

P-wave parameters versus S-wave amplitude

Pa vs. S-wave amplitude

The initial set of relationships analysed focused on P-wave Pa values and their correlation with S-wave amplitude parameters, including PGA, PGV, and PGD (Fig. 3).

The relationship between P-wave amplitude (Pa) and S-wave amplitude measured by PGA demonstrates a strong correlation. As depicted in Fig. 3a, the empirical relationship (Eq. 1 from Table 4) produced R and R^2 values of 0.891 and 0.793, indicating a robust association. This high R^2 suggests that the variability in Pa substantially explains the variance in PGA values. The RMSE of 0.296 and a 5-fold Cross-validation RMSE ranging from 0.251 to 0.384 confirm the model's accuracy and consistency.

Regarding the P-wave amplitude (Pa) compared with the S-wave's PGV, Fig. 3b showcases the Pa versus PGV relationship (Eq. 2 from Table 4), yielding R and R² values of 0.872 and 0.760, respectively. Although slightly lower than the Pa-PGA relationship, these figures still represent a significant correlation, indicating that Pa variations can explain a large portion of the PGV variability. The RMSE for this relationship is 0.349, with the 5-fold Cross-validation RMSE values ranging from 0.291 to 0.512, reflecting the model's reliability across different subsets of data.

Table 3 Assigned weights and justification for performance metrics in linear regression model selection

Metric	Weight
Trained R^2	0.1
Tested R^2	0.1
Trained RMSE	0.2
Tested RMSE	0.3
Mean of 5-fold Cross-validation RMSE	0.6

Finally, the analysis of Pa against the S-wave amplitude measured by PGD is shown in Fig. 3c. The empirical relationship (Eq. 3 from Table 4) resulted in R and R² values of 0.835 and 0.697, respectively. These values indicate a strong but less pronounced correlation compared to the earlier relationships. The RMSE of 0.395 and the 5-fold Cross-validation RMSE values between 0.310 and 0.609 suggest a slightly greater deviation from the model predictions, highlighting the challenges in predicting PGD from Pa.

Pv vs S-wave amplitude

The subsequent analysis explored relationships involving Pv values for P-waves and the S-wave amplitude measured as PGA, PGV, and PGD. Figure 4 illustrates the obtained graphs for the Pv vs. PGA, Pv vs. PGV, and Pv vs. PGD relationships.

As depicted in Fig. 4a, the relationship between Pv and PGA (Eq. 4 from Table 5) exhibited a robust positive correlation, with R and R² values of 0.914 and 0.835, respectively. These high R and R² values, surpassing those seen in relationships involving Pa, indicate a more consistent and robust predictive capability. The RMSE of 0.266 and the

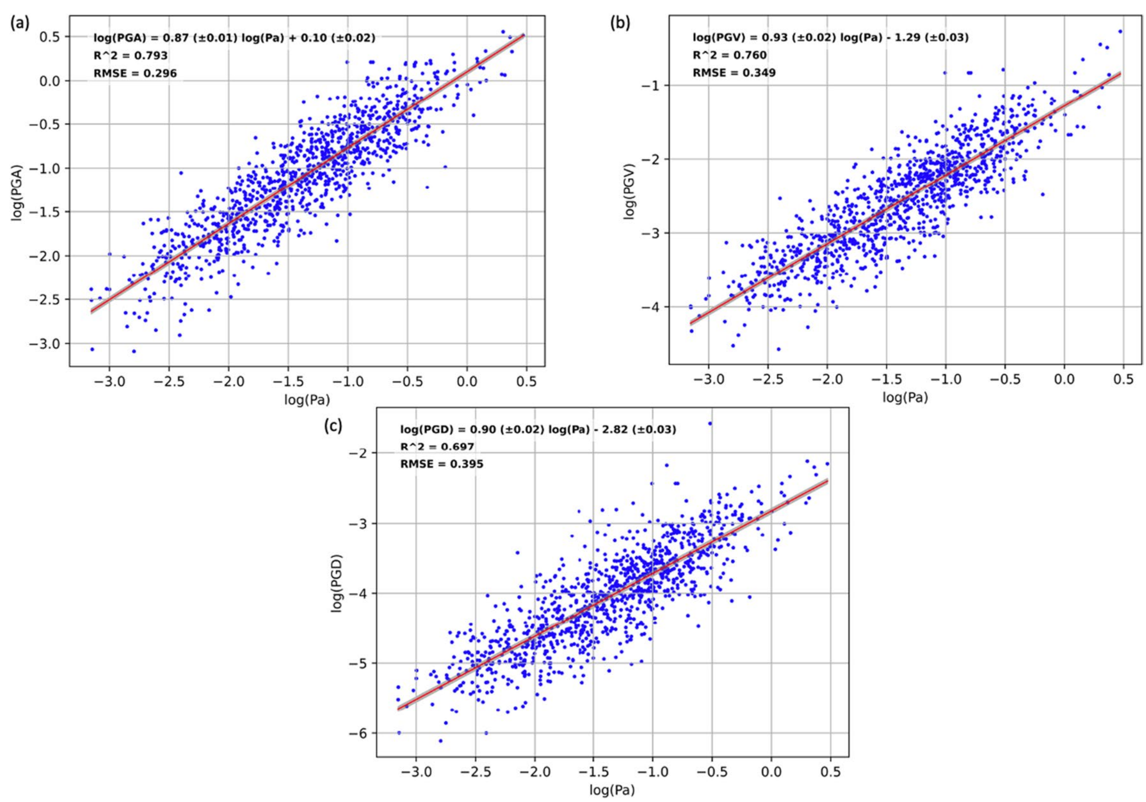

Fig. 3 Empirical relationships between P-wave Pa and S-wave parameters for Site Class D. Panel (**a**) shows Pa vs. PGA, (**b**) shows Pa vs. PGV, and (**c**) shows Pa vs. PGD. Each graph features data points in blue, a linear regression line in red, and the 95% confidence interval shaded in grey

Table 4 Summary of empirical relationships, R, R2, RMSE and 5-fold cross-validation RMSE values obtained for P-wave's Pa and S-wave amplitude parameters (PGA, PGV and PGD)

Equation	Parameters	Empirical relationship	R	R^2	RMSE	5-fold Cross-validation RMSE
1	Pa Vs PGA	log (PGA) = 0.87 (±0.01) log (Pa) + 0.10 (±0.02)	0.891	0.793	0.296	[0.384, 0.279, 0.262, 0.251, 0.36]
2	Pa Vs PGV	log (PGV) = 0.93 (±0.02) log (Pa) – 1.29 (±0.03)	0.872	0.760	0.349	[0.45, 0.321, 0.291, 0.293, 0.512]
3	Pa Vs PGD	log (PGD) = 0.90 (±0.02) log (Pa) – 2.82 (±0.03)	0.835	0.697	0.395	[0.518, 0.345, 0.319, 0.31, 0.609]

5-fold Cross-validation RMSE ranging from 0.226 to 0.33 further underscore the model's accuracy and consistency.

The empirical analysis extended to the relationship between Pv and PGV, as illustrated in Fig. 4b. This relationship (Eq. 5 from Table 5) yielded similar R and R² values of 0.914 and 0.835, respectively, demonstrating a robust positive correlation. This reflects the same level of consistency as the Pv versus PGA analysis despite a marginally higher RMSE of 0.290 and a 5-fold Cross-validation RMSE between 0.253 and 0.407.

Finally, Fig. 4c highlights the Pv versus PGD relationship (Eq. 6 from Table 5), which recorded R and R² values of 0.875 and 0.765. These values, while strong, are slightly lower than those of the previous Pv relationships. The RMSE of 0.349 and a 5-fold Cross-validation RMSE ranging from 0.286 to 0.517 suggest a more noticeable variability between observed and predicted values, reflecting the challenges in predicting PGD from Pv with the same precision as PGA or PGV.

Pd vs S-wave amplitude

The final set of analyses investigates the empirical relationships between P-wave amplitude, represented by Pd, and S-wave amplitudes, represented by PGA, PGV, and PGD. Figure 5 provides a graphical visualisation of the computed relationships, illustrating the interaction between these seismic parameters.

The relationship between Pd and PGA (Eq. 7 from Table 6) demonstrated a robust positive correlation, with R

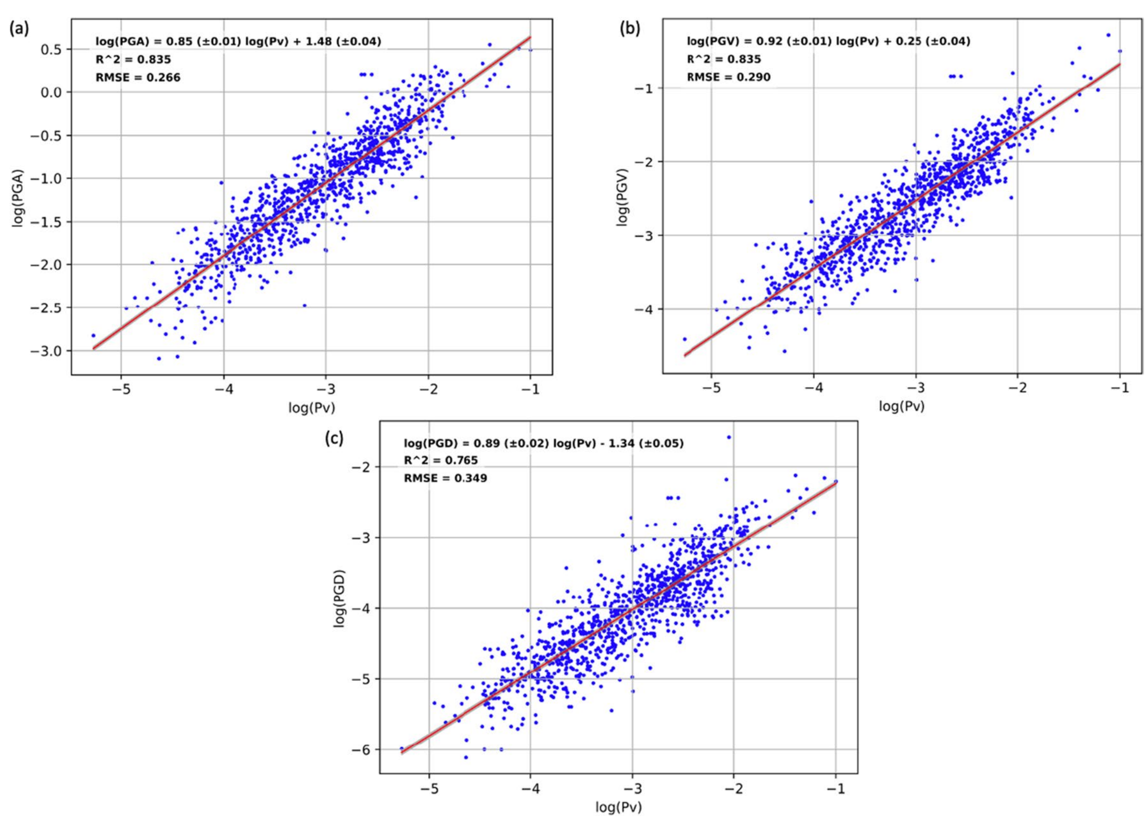

Fig. 4 Empirical relationships between P-wave Pv and S-wave parameters for Site Class D. Panel (**a**) shows Pv vs. PGA, (**b**) shows Pv vs. PGV, and (**c**) shows Pv vs. PGD. Each graph features data points in blue, a linear regression line in red, and the 95% confidence interval shaded in grey

and R^2 values of 0.902 and 0.814, respectively, as shown in Fig. 5a. This relationship exhibited an RMSE of 0.280, with a 5-fold Cross-validation RMSE ranging between 0.239 and 0.351. These metrics suggest a firm consistency and reliability in predicting PGA from Pd.

Further, the relationship between Pd and PGV is explored and is depicted in Fig. 5b. This relationship (Eq. 8 from Table 6) produced R and R^2 values of 0.920 and 0.846, respectively, indicating an even stronger positive correlation than the Pd vs. PGA relationship. The RMSE is slightly lower at 0.279, with a 5-fold Cross-validation RMSE between 0.243 and 0.349, reinforcing the model's accuracy in predicting PGV from Pd.

Lastly, Fig. 5c depicts the relationship between Pd and PGD (Eq. 9 from Table 6), yielding R and R^2 values of 0.911 and 0.830, respectively. These values suggest a substantial predictive capability, although slightly reduced compared to the Pd vs. PGV relationship. The RMSE for this relationship is 0.295, with a 5-fold Cross-validation RMSE spanning from 0.254 to 0.389, indicating slightly higher variability in predictions for PGD relative to PGA and PGV.

Evaluation of error distribution for S-wave amplitude estimation

The residuals from each of the nine empirical relationships are analysed to evaluate the error distribution for the S-wave amplitude estimation. The analysis included calculating the Mean error, Median error, Standard Deviation, and Mean Absolute Error (MAE) for the residuals, in addition to the RMSE. Table 7 summarises the values obtained from these calculations.

The error distribution analysis for S-wave amplitude estimation reveals that the mean and median errors are minimal and negligible across all models, indicating that the residuals are centred around zero.

- Standard Deviation: The Pv vs. PGA model exhibits the lowest standard deviation (0.2655), indicating greater consistency in its residuals. In contrast, the Pa vs. PGD model shows the highest standard deviation (0.395), indicating higher variability.
- MAE: The Pv vs. PGA model has the lowest MAE of 0.2046, highlighting its accuracy and reliability. Other notable performances include the Pd vs. PGA model, which has an MAE of 0.2063, and the Pd vs. PGV model, which has an MAE of 0.2068.

The Pv vs. PGA model consistently demonstrates better performance regarding Standard Deviation, and MAE. Other models, such as Pv vs. PGV and Pd vs. PGA, also show strong performance, particularly the MAE, highlighting their potential effectiveness in predicting S-wave amplitudes. Further, histograms that show the frequency distribution of residuals in estimating S-wave amplitudes are plotted for each of the nine relationships and attached in the Appendix as Fig. 13.

Evaluation and generalisation of the linear regression relationships with testing data

This section details the evaluation results of the constructed linear regression models using the testing dataset.

Table 8 summarises the R^2 (Tested R^2) and RMSE (Tested RMSE) values for each relationship, comparing the outcomes from the training phase and those observed with the testing phase.

Among the evaluated relationships, the Pv vs. PGA relationship exhibited superior performance, achieving the highest R^2 of 0.716, which indicates a strong correlation and predictive capability, along with the lowest RMSE of 0.305, suggesting minimal prediction errors. In contrast, the Pa vs. PGD relationship showed the least predictive accuracy, with the lowest R^2 of 0.392 and the highest RMSE of 0.471, indicating higher prediction variability.

Furthermore, relationships involving Pd in overall demonstrated commendable performance, with the Pd vs. PGA relationship being notably effective, achieving an R^2 of 0.699 and an RMSE of 0.314. In contrast, relationships based on Pa generally showed poorer performance, as evidenced by lower R^2 values and higher RMSEs across the board, indicating a reduced reliability for making precise predictions.

Table 5 Summary of empirical relationships, R, R2, RMSE and 5-fold cross-validation RMSE values obtained for P-wave's pv and S-wave amplitude parameters (PGA, PGV and PGD)

Equation	Parameters	Empirical relationship	R	R^2	RMSE	5-fold Cross-validation RMSE
4	Pv Vs PGA	log (PGA) = 0.85 (±0.01) log (Pv) + 1.48 (±0.04)	0.914	0.835	0.266	[0.33, 0.239, 0.257, 0.226, 0.297]
5	Pv Vs PGV	log (PGV) = 0.92 (±0.01) log (Pv) + 0.25 (±0.04)	0.914	0.835	0.290	[0.355, 0.263, 0.264, 0.253, 0.407]
6	Pv Vs PGD	log (PGD) = 0.89 (±0.02) log (Pv) – 1.34 (±0.05)	0.875	0.765	0.349	[0.425, 0.313, 0.31, 0.286, 0.517]

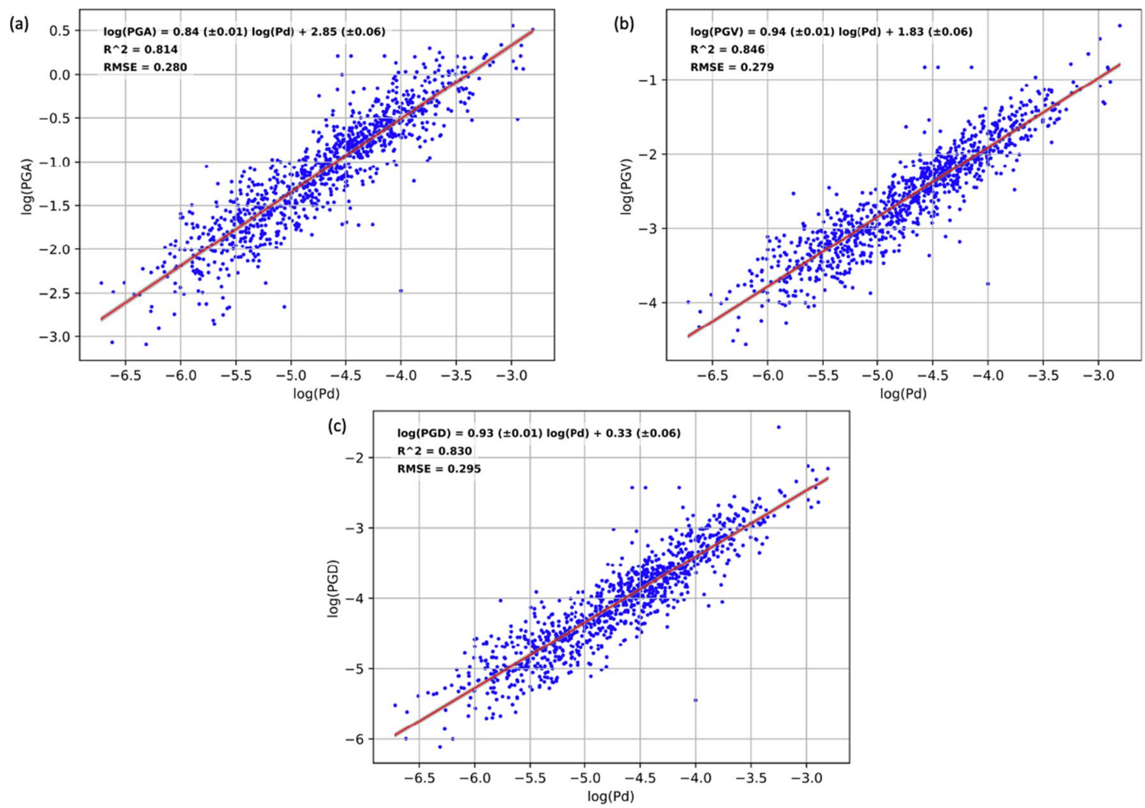

Fig. 5 Empirical relationships between P-wave Pd and S-wave parameters for Site Class D. Panel (**a**) shows Pd vs. PGA, (**b**) shows Pd vs. PGV, and (**c**) shows Pd vs. PGD. Each graph features data points in blue, a linear regression line in red, and the 95% confidence interval shaded in grey

Table 6 Summary of empirical relationships, R, R2, RMSE and 5-fold cross-validation RMSE values for P-wave's pd and S-wave amplitude parameters (PGA, PGV and PGD)

Equation	Parameters	Empirical relationship	R	R^2	RMSE	5-fold Cross-validation RMSE
7	Pd Vs PGA	log (PGA) = 0.84 (±0.01) log (Pd) + 2.85 (±0.06)	0.902	0.814	0.280	[0.351, 0.258, 0.239, 0.239, 0.313]
8	Pd Vs PGV	log (PGV) = 0.94 (±0.01) log (Pd) + 1.83 (±0.06)	0.920	0.846	0.279	[0.33, 0.258, 0.243, 0.254, 0.349]
9	Pd Vs PGD	log (PGD) = 0.93 (±0.01) log (Pd) + 0.33 (±0.06)	0.911	0.830	0.295	[0.369, 0.266, 0.262, 0.254, 0.389]

Table 7 Summary of error distribution metrics for S-wave amplitude estimation, including mean error, median error, standard deviation, range, and MAE for each of the nine empirical relationships

Model	Median error	Standard Deviation	MAE
Pa vs. PGA	0.0121	0.296	0.234
Pa vs. PGV	0.0039	0.346	0.2763
Pa vs. PGD	-0.0022	0.395	0.3054
Pv vs. PGA	0.0186	0.2655	0.2046
Pv vs. PGV	0.0085	0.2904	0.2235
Pv vs. PGD	0.0103	0.349	0.2651
Pd vs. PGA	0.0109	0.2801	0.2063
Pd vs. PGV	-0.0024	0.2788	0.2068
Pd vs. PGD	-0.0057	0.2953	0.2213

Identifying overfitting and underfitting in linear regression models

This section outlines the results concerning the analysis of overfitting and underfitting within the constructed linear regression models.

Overfitting in linear regression models is characterised by high R^2 values during training with a substantial test drop, suggesting the model memorises specifics rather than generalises. This is further indicated by low training RMSEs that increase significantly during testing and inconsistent performance across different subsets in 5-fold Cross-validation RMSE (Tigran 2022; Will Koehrsen 2018).

Table 8 Comparison of trained and tested R² and RMSE values for the nine linear regression relationships

Relationship	Trained model		Tested model	
	R^2	RMSE	R2	RMSE
Pa vs. PGA	0.793	0.296	0.639	0.343
Pa vs. PGV	0.760	0.349	0.453	0.411
Pa vs. PGD	0.697	0.395	0.392	0.471
Pv vs. PGA	0.835	0.266	0.716	0.305
Pv vs. PGV	0.835	0.290	0.618	0.343
Pv vs. PGD	0.765	0.349	0.573	0.394
Pd vs. PGA	0.814	0.280	0.699	0.314
Pd vs. PGV	0.846	0.279	0.626	0.339
Pd vs. PGD	0.830	0.295	0.632	0.366

Conversely, underfitting is marked by uniformly low R² and high RMSE across training and testing phases, reflecting the model's failure to capture essential data trends. Elevated Cross-validation RMSEs also underscore underfitting, revealing the model's inadequate performance on unseen segments of the training data (Tigran 2022; Will Koehrsen 2018).

The analysis of the constructed relationships using the calculated metrics provides a clear indication of their varying abilities to model and predict unseen data effectively:

- Relationships with Pa: The Pa vs. PGA and Pa vs. PGV models exhibit signs of overfitting. While their Trained R2 values are relatively high (0.793 and 0.76, respectively), the significant drop in R2 and increase in RMSE when moving to the test dataset (0.639 vs. 0.343 for Pa vs. PGA and 0.453 vs. 0.411 for Pa vs. PGV) suggest the models are not generalising well to unseen data. The Pa vs. PGD model shows even stronger evidence of overfitting, with a very low Tested R2 (0.392) and high Tested RMSE (0.471).
- Relationships with Pv: The Pv vs. PGA model demonstrates the best overall performance. Its Trained and Tested R2 values are high (0.835 and 0.716, respectively), and the increase in Tested RMSE (0.305) is moderate. The 5-fold Cross-validation RMSE also suggests good generalisability, indicating that the model captures the underlying relationship effectively and performs well on unseen data. The Pv vs. PGV and Pv vs. PGD models show similar trends, although with slightly lower performance than Pv vs. PGA.
- Relationships with Pd: The Pd vs. PGA, Pd vs. PGV, and Pd vs. PGD models exhibit good performance. Their Trained and Tested R2 values are high (above 0.8 for Trained R2 and above 0.6 for Tested R2), and the increases in Tested model RMSE are moderate. The 5-fold Cross Validation RMSE values also indicate good generalisability.

Evaluating linear regression relationships through weighted scoring

As outlined in the "Method" section, the weighted scores for each constructed relationship are computed using Formula 3. The following table (Table 9) presents the results derived from the weighted scoring approach, quantifying the efficacy of various relationships in estimating S-wave amplitude from P-wave amplitude.

The analysis revealed a prominent relationship between Pv and PGA, evidenced by the highest weighted score of 1.29. This association stood out due to its strong correlation and consistent predictive ability, suggesting its potential value as a model within EEWSs. Conversely, relationships involving Pa displayed lower efficacy. This is reflected in their weighted scores: Pa vs. PGA (0.98), Pa vs. PGV (0.43), and particularly Pa vs. PGD (0.0), which suggests minimal utility in employing Pa for accurate S-wave prediction. Additionally, Pd-related relationships demonstrated positive performance, with Pd vs. PGA and Pd vs. PGV achieving scores of 1.19 and 1.12, respectively. These scores indicate strong reliability in utilising Pd parameters for estimating S-wave amplitude, although they are surpassed by the Pv vs. PGA relationship.

Discussion

This research has evaluated different P-wave parameters for estimating S-wave amplitude in EEWS, assessing their effectiveness and generalisability. The findings indicate that Pv is the most suitable parameter for estimating S-wave amplitude, especially for PGA, a crucial indicator of ground shaking. Additionally, Pd shows robust performance, whereas Pa displays certain limitations. The subsequent section will further explore these results and discuss their broader implications.

Efficacy of Pd in predicting S-wave amplitude The correlation between P-wave amplitude and S-wave amplitude is comprehensively analysed using the metrics R, R², RMSE, and 5-fold Cross-validation RMSE for the nine developed models. The Pd parameter consistently demonstrated robust predictive power across its relationships

Table 9 Weighted scores for assessing the efficacy of linear regression relationships in estimating s-wave amplitude from p-wave amplitude

Equation	Relationship	Weighted score
1	Pa vs. PGA	0.98
2	Pa vs. PGV	0.43
3	Pa vs. PGD	0
4	Pv vs. PGA	1.29
5	Pv vs. PGV	1
6	Pv vs. PGD	0.51
7	Pd vs. PGA	1.19
8	Pd vs. PGV	1.12
9	Pd vs. PGD	0.96

with S-wave amplitudes, notably PGA, PGV, and PGD. It exhibited strong correlations, with R values exceeding 0.9 and R^2 values of 0.814, 0.846, and 0.83, respectively, indicating significant predictive capabilities (Table 6). Furthermore, RMSE values for these relationships remained uniformly low, below 0.3, underscoring their prediction accuracy. The 5-fold Cross-validation RMSE results further reinforced the reliability of the Pd-based models, with values ranging from 0.239 to 0.389, indicating good generalisation performance. These metrics collectively affirm Pd's efficacy as a dependable predictor of S-wave amplitude, reinforcing its value in EEWSs.

Limitations of Pa in predicting S-wave amplitude Empirical relationships utilising Pa to predict S-wave amplitudes exhibited considerably poorer fits, reflecting findings similar to those reported in studies on EEWSs employing MEMS sensors, such as the research conducted by Wu et al. (2005b). Specifically, when estimating S-wave amplitudes (PGA, PGV, and PGD) using Pa, the relationships demonstrated lower R and R^2 values and higher RMSEs, indicating a less accurate fit. The 5-fold Cross-validation RMSE values further revealed higher prediction errors across all folds for these three S-wave amplitude predictions, underscoring the models' inadequacies. Notably, the relationship between Pa and PGD is weak, recording the lowest R and R^2 values of 0.835 and 0.697, respectively, and the highest RMSE at 0.395. Cross-validation RMSEs for this relationship varied from 0.319 to 0.609, indicating substantial prediction errors and poor generalisability to new data. These results highlight the limited effectiveness of Pa as a predictor of S-wave amplitude, especially in estimating PGD.

Pv as the optimal predictor for S-wave amplitude Despite not reaching the highest correlation levels achieved by Pd models, Pv has shown robust overall correlations as a predictor of S-wave amplitudes. The relationships involving Pv and various S-wave parameters—PGA, PGV, and PGD—demonstrate strong statistical correlations, with R values consistently above 0.85 and R^2 values exceeding 0.75. Particularly notable are the Pv versus PGA and Pv versus PGV models, which recorded R and R^2 values of 0.914 and 0.835, respectively. These high metrics signify strong linear associations between Pv and S-wave amplitudes.

The Pv vs. PGA model, with its low RMSE of 0.266, stands out among the Pv relationships, indicating minimal prediction error, reflecting the model's accuracy in estimating PGA from Pv. Moreover, the 5-fold Cross-validation RMSE results further validate the reliability of the Pv-based models. The consistently low error rates across all folds highlight excellent generalisability to new, unseen data. Additionally, the error distribution analysis of S-waves indicated that the Pv vs. PGA model consistently demonstrates better performance regarding Standard Deviation and MAE than other models. These findings solidify Pv's status as an effective and dependable indicator of S-wave amplitude, particularly for predicting PGA, and underscore its practical implications in real-world scenarios.

Testing data evaluation Evaluating the constructed models with a test dataset spanning 2020 to 2023 is a pivotal step in assessing the generalisability and robustness of the linear regression models. As shown in Table 7, the Pv vs. PGA relationship stands out with the highest R^2 of 0.716 for the test dataset. It underscores its strong correlation and predictive capability alongside the lowest RMSE of 0.305, indicating minimal prediction errors. However, it contrasts with the Pa vs. PGD relationship, which exhibited the lowest tested R^2 of 0.392 and the highest RMSE of 0.471, highlighting considerable prediction variability. Further, relationships involving Pd overall showed commendable performance, with the Pd vs. PGA relationship notably achieving an R^2 of 0.699 and an RMSE of 0.314, demonstrating its effectiveness.

Pv and Pd avoid overfitting and underfitting While the relationships with Pv and Pd demonstrated significant correlations with S-wave amplitudes, understanding their modelling characteristics regarding overfitting and underfitting is crucial (Section 4.3). For instance, relationships involving Pa, such as Pa vs. PGA, Pa vs. PGV and Pa vs. PGD, exhibited overfitting with substantial drops in R^2 and increases in RMSE, suggesting poor generalisation. Conversely, the Pv vs. PGA relationship showed robust performance with high R^2 values and moderate RMSE increases during testing, underscoring its effective learning and generalisation capabilities. Similarly, models involving Pd, such as Pd vs. PGA, maintained high R^2 and moderate RMSE increases, indicating robust learning and predictive reliability. These insights highlight the potential of Pv and Pd parameters in providing reliable predictions in real-world settings, with the Pv vs. PGA model marked as the most effective based on the measured metrics.

Rationale behind Pa's poor performance and pv and pd's effective predictive capabilities The observed poor correlation when using Pa as the amplitude parameter for the initial motion can be attributed to its susceptibility to misinterpretations, especially in the context of nearby small seismic events. Pa may yield comparatively large values for such events, even though the resulting PGA and PGV values are relatively small. This discrepancy arises due to differences in frequency content and attenuation. Pa primarily reflects the characteristics of a very high-frequency seismic wave, which attenuates more rapidly with distance and, therefore, has a lower potential for causing significant damage. In contrast, Pv and Pd capture lower frequency content, which attenuates less rapidly and is more indicative of the seismic energy that can cause considerable damage (Wu and Kanamori 2005b). Therefore, Pv and Pd correlate strongly with critical seismic amplitude indicators like PGA and PGV. Notably, Pd demonstrates a notable correlation with peak amplitude parameters, which is pivotal in assessing the seismic impact (Wu and Kanamori 2005b). Another critical factor is the integration process used to determine Pv and Pd. This process acts as a natural low-pass filter, smoothing out high-frequency noise and providing a more stable signal. This stability is crucial for accurate prediction models, as it reduces the likelihood of overfitting to noise and local site effects in the initial P-wave data. Therefore, using Pa as the triggering parameter in an EEW network is limited since it could lead to an increased occurrence of false alerts, undermining the effectiveness of the EEWS.

Results comparison to prior research To further contextualise the findings, a comparative analysis is conducted between the results of this study and those reported in previous research papers that have explored empirical relationships. This study comprehensively compares various relationships between P-wave and S-wave amplitude parameters, enhancing the understanding of seismic predictors by detailing how different P-wave parameters correlate with S-wave amplitudes across various scenarios. In contrast, much of the literature, such as the studies by Wang et al. (2020) and Wu and Kanamori (2005b) have focused on specific relationships like Pd vs. PGV.

For instance, a study by Wu and Kanamori (2008) in Taiwan, which used 780 records to establish a relationship between Pd and PGV, reported a standard deviation (SDV) of 0.326 but did not specify R or R^2 values; similarly, Wu and Mittal (2021) investigated this relationship using earthquake recordings from Japan, Taiwan, and Southern California, reporting an R-value of 0.873 and an SDV of 0.326, which is slightly lower than this study's R-value of 0.920 and RMSE of 0.279 for the Pd vs. PGV model. Caruso et al. (2017) built a relationship between Pd and PGV using Italian earthquake data, resulting in an R^2 of 0.760 and an SDV of 0.36, which compares to the R^2 of 0.846 reported in this study for the same relationship, although with a slightly lower RMSE of 0.279. These comparisons highlight the robustness of the empirical relationships established in the current research within the context of NZ earthquake data, underscoring the comparative performance of these models against international studies. However, direct comparisons are complicated by some studies not reporting all metrics such as R, R^2, or RMSE, which underscores the need for standardised reporting in seismic research.

Weighted scoring approach to identify optimal model In this study, the challenge of comparing linear regression models, particularly between Pv and Pd relationships, necessitated a method that could systematically evaluate and select the optimal model. These models often yield similar results, making it difficult to discern the most effective one for EEW applications. To address this, the weighted scoring method is introduced (Griffith and Headley 1997). This approach allows for an objective comparison by focusing on crucial metrics from an EEW perspective. By assigning weights to different performance metrics, such as R^2 and RMSE (see Formula 3), and evaluating them in a structured manner, this method helps prioritise models that are statistically robust and most relevant for practical implementation in seismic alert systems.

Among the assessed models (Table 8 provides a clear summary of these scores), the relationship between Pv and PGA stood out significantly, achieving the highest weighted score of 1.29. This score reflects its robust correlation and consistent predictive accuracy, marking it as a highly effective model within EEWSs. Conversely, models involving Pa, such as Pa vs. PGV and Pa vs. PGD, exhibited much lower effectiveness, with scores of 0.43 and 0, respectively, indicating their limited utility in accurate S-wave prediction. Meanwhile, Pd-related models displayed strong performance, with scores of 1.19 for Pd vs. PGA and 1.12 for Pd vs. PGV, demonstrating their reliability in estimating S-wave amplitude, albeit not surpassing the superior performance of the Pv vs. PGA relationship.

In conclusion, the study identifies the empirical relationship between Pv and PGA as the most suitable for estimating S-wave amplitude for the Canterbury region of NZ, demonstrating superior performance across training and testing datasets. This relationship's robustness is critical for the real-time application of EEWS, providing a reliable basis for operational success. Additionally, the chosen relationship enhances the integration of the S-wave-based PLUM algorithm with the P-wave detection algorithm, effectively reducing the inherent limitations of the PLUM algorithm's warning time. As outlined in the case study below, this relationship is also crucial in establishing a P-wave amplitude threshold. By setting a critical Pv value threshold, the EEWS can trigger alerts when this value is exceeded, indicating potential significant ground shaking.

Case study: establishing EEW alert threshold for earthquakes in Canterbury

The study presents a case study showcasing the application of the selected empirical relationship in determining the threshold for felt earthquakes. The case study aims to establish the Pv threshold that would enable the issuance of alerts for a level of shaking that would be felt in the Canterbury region of NZ. This application uses the new Ground Motion to Intensity Conversion Equations (GMICEs) (Moratalla et al. 2020) constructed for NZ to derive the Pv threshold.

Method

MMI selection The initial step involves selecting a Modified Mercalli Intensity (MMI) range suitable for EEW purposes. This range determines the ground-shaking intensity levels that necessitate issuing an alert. For this selection, the study references the MMI descriptions provided by GeoNet (Dowrick 1996; Dowrick et al. 2008). This ensures alignment with the regional seismic conditions and enhances the relevance of our chosen MMI range.

S-wave parameter threshold identification To determine the threshold value for the S-wave PGA, we use Moratalla et al. (2020) study which introduced new GMICEs designed explicitly for NZ. This study established relationships between the earthquakes' MMI scale and PGA values. By plotting this relationship, the PGA value associated with perceivable ground shaking in the chosen MMI range can be identified. This value is then employed as the S-wave threshold to indicate felt ground shaking.

P-wave parameter threshold derivation Utilising the selected empirical relationship between Pv and PGA, the corresponding threshold value for the P-wave parameter (Pv) is calculated based on the identified S-wave parameter (PGA) threshold.

Results

According to the GeoNet MMI description (Dowrick 1996; Dowrick et al. 2008), an MMI value of 5 is selected as the threshold for EEW activation. This level represents shaking generally felt outdoors, awakens most sleepers, and may alarm some individuals indoors.

PGA values corresponding to an MMI of 5 are calculated using the GMICEs (Formula 4 and 5) provided by Moratalla et al. (2020). Figure 6 graphically depicts the relationship between MMI and PGA, where the chosen MMI threshold of 5, relevant to EEW generation, is indicated with a green vertical line.

$$\log(\mathrm{PGA}) = (\mathrm{MMI} - 1.7601)/1.992 \text{ if } \mathrm{MMI} < 5.5277 \tag{4}$$

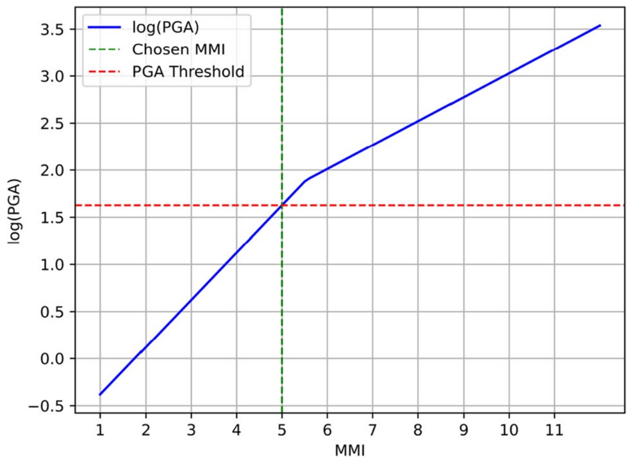

Fig. 6 Relationship between MMI and PGA using GMICEs (1) and (2) as provided by Moratalla et al. (2020). The vertical green line represents the selected MMI value (MMI 5), and the horizontal red line indicates the PGA threshold for perceivable ground shaking

$$\log(\mathrm{PGA}) = (\mathrm{MMI} + 1.9095)/3.9322 \text{ if } \mathrm{MMI} \geq 5.5277 \tag{5}$$

PGA threshold identification The corresponding log (PGA) threshold for S-waves is identified by examining the intersection point on the graph depicted in Fig. 6. At this juncture, the log (PGA) value, determined as the threshold for S-waves, is 1.63, as indicated by the red dashed horizontal line on the graph. Upon converting this logarithmic value back to its original scale, the PGA threshold is established at 42.3 cm^{-2}.

Pv threshold derivation Following the identification of the PGA threshold, this value is applied to the selected empirical relationship, defined as log (PGA) = 0.85 (±0.01) log (Pv) + 1.48 (±0.04), to derive the corresponding Pv threshold for event detection. This process established a Pv threshold ranges between 0.6 and 0.8 cm^{-1} according to the uncertainty in the linear regression coefficients. Selecting a Pv threshold of 0.6 cm^{-1} is considered most suitable, as a higher threshold may increase the risk of missed alerts, a critical concern in EEWSs.

When the Pv exceeds 0.6 cm^{-1}, the event is highly likely to be felt. Implementing a Pv threshold at 0.6 cm^{-1} would have enabled the EEWS to issue alerts for perceivable earthquake events. This threshold is applicable both in on-site EEWSs, where individual stations operate independently to issue warnings and in regional EEWSs, where data from multiple stations are aggregated to issue warnings.

This application's MMI value (5 or above) choice for triggering EEW alerts is grounded in GeoNet's MMI description. This approach serves as an illustrative example, showcasing the practicality of the selected relationship for EEW purposes with a specific focus on MMIs indicative of significant seismic events. The selection of the MMI value potentially leads to debates among social and technical scientists regarding the most suitable threshold for generating alerts using the detected P-wave 3-second window. The ability to customise the threshold based on unique regional characteristics and priorities remains a valuable consideration.

Limitations and future work

While providing valuable insights into P and S-wave amplitude relationships for NZ based on data from the Canterbury region, the study has certain limitations and opens avenues for future research.

The study's data source primarily relies on ground motion data from the CanNet network, which utilises MEMS-based sensors. This aligns with the implementation of the CRISiSLab EEW network. Future work aims to extend the analysis by incorporating a more extensive dataset from GeoNet's strong motion sensors, providing a broader spectrum of ground motion data across NZ. Including more data will facilitate the exploration of complex machine learning-based models to construct more nuanced and accurate relationships for S-wave amplitude, thereby enhancing the precision and effectiveness of the EEWS. This expansion will also allow for a more comprehensive investigation into the P and S-wave amplitude relationships, addressing the current data source's limitations and broadening the research scope. Further, it is important to note that the results from this study are not compared with machine learning-based approaches found in the literature, as it would not be a fair comparison due to the differences in dataset sizes and complexities. Future work with a larger dataset will enable a more equitable evaluation of the performance metrics between linear regression and machine learning models.

This study's analysis considered stations installed within a single Site Class to maintain consistent soil characteristics throughout. Future research plans to expand the study to include different Site Classes within NZ. This expansion will provide a more comprehensive understanding of regional variability in P and S-wave amplitude relationships, contributing to the findings' generalisability and enhancing the EEWS's applicability across diverse geological settings.

Conclusion

This study makes a significant contribution by comprehensively comparing various relationships between P-wave and S-wave amplitude parameters, distinguishing itself from prior studies that often focused on singular or limited relationships. Among the various relationships examined, it is evident that Pv exhibited a strong and dependable correlation with PGA.

This research marks a crucial step towards establishing a robust, low-cost EEWS in NZ. Having implemented a community-engaged, low-cost EEW network in NZ (Prasanna et al. 2022), the findings will be the basis for linking detected P-waves to impending ground shaking caused by S-waves. It facilitates the integration of the S-wave-based PLUM algorithm with the P-wave detection algorithm, effectively overcoming the limited warning time inherent to the PLUM algorithm. As shown in the case study, this relationship provides a foundational element for determining the suitable threshold for EEW alerts, enhancing the system's overall responsiveness and reliability.

By choosing Pv vs. PGA as the suitable relationship, we showcased its practicality by setting a threshold for the selected P-wave parameter (Pv) that triggers EEW alerts in the Canterbury region of NZ, employing an application using GMICEs. This case study approach is particularly tailored to detecting earthquakes resulting in perceivable ground shaking within the Canterbury region of NZ. However, the approach used in this study is more comprehensive than the specific use case presented; it holds the potential for application and extension to other regions in NZ or areas with similar seismic characteristics. Furthermore, employing this approach to establish empirical relationships between P and S-wave amplitudes for other regions enables the determination of thresholds for detecting ground shaking, enhancing the effectiveness of an EEWS tailored to specific geographic locations and seismic conditions.

This study has laid the foundation for establishing a relationship between P and S-wave amplitudes for EEW, contributing to improved seismic hazard mitigation in NZ. There are opportunities for future research on prioritising the expansion of the ground motion dataset and exploring complex machine learning-based techniques for predicting S-wave amplitude. The insights gained from this study provide a valuable resource for enhancing the accuracy and timeliness of EEW in NZ, ultimately safeguarding lives and property during seismic events.

Appendix

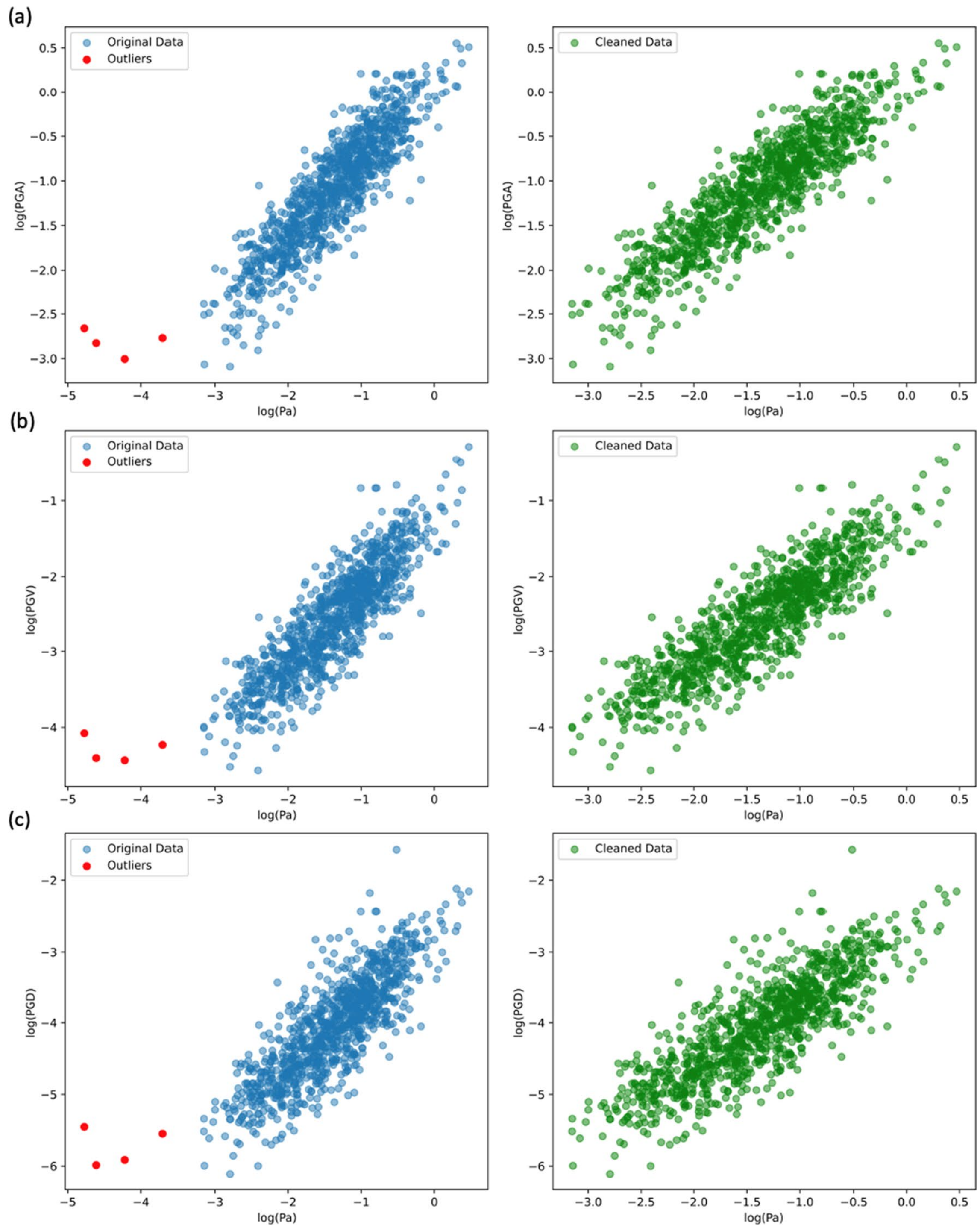

Fig. 7 It shows the original and cleaned training data for relationships using Pa as the input parameter. Panel (**a**) displays Pa vs. PGA, panel (**b**) shows Pa vs. PGV, and panel (**c**) depicts Pa vs. PGD, with each panel comparing original data (left) and data post-outlier removal (right)

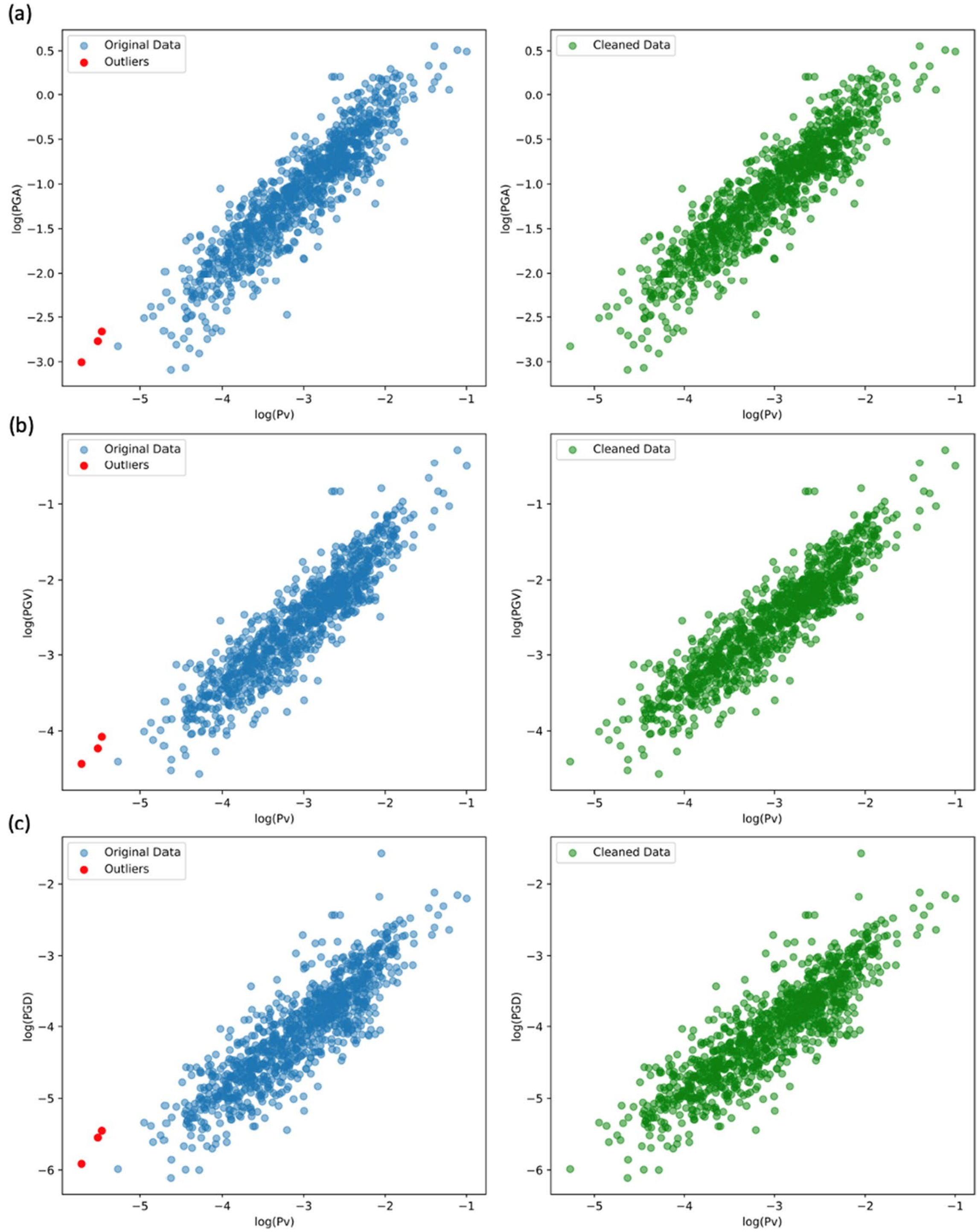

Fig. 8 It shows the original and cleaned training data for relationships using Pv as the input parameter. Panel (**a**) displays Pv vs. PGA, panel (**b**) shows Pv vs. PGV, and panel (**c**) depicts Pv vs. PGD, with each panel comparing original data (left) and data post-outlier removal (right)

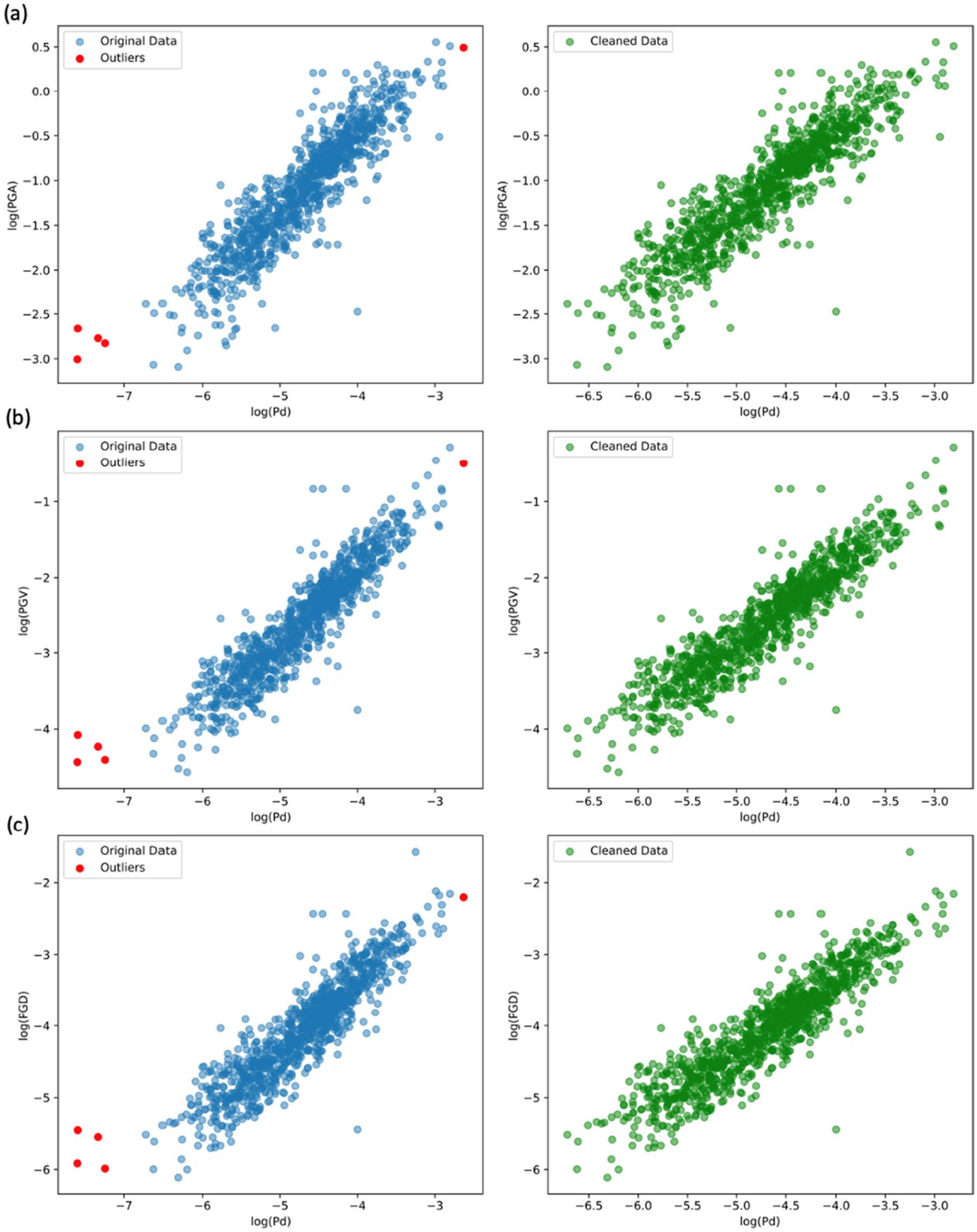

Fig. 9 It shows the original and cleaned training data for relationships using Pd as the input parameter. Panel (**a**) displays Pd vs. PGA, panel (**b**) shows Pd vs. PGV, and panel (**c**) depicts Pd vs. PGD, with each panel comparing original data (left) and data post-outlier removal (right)

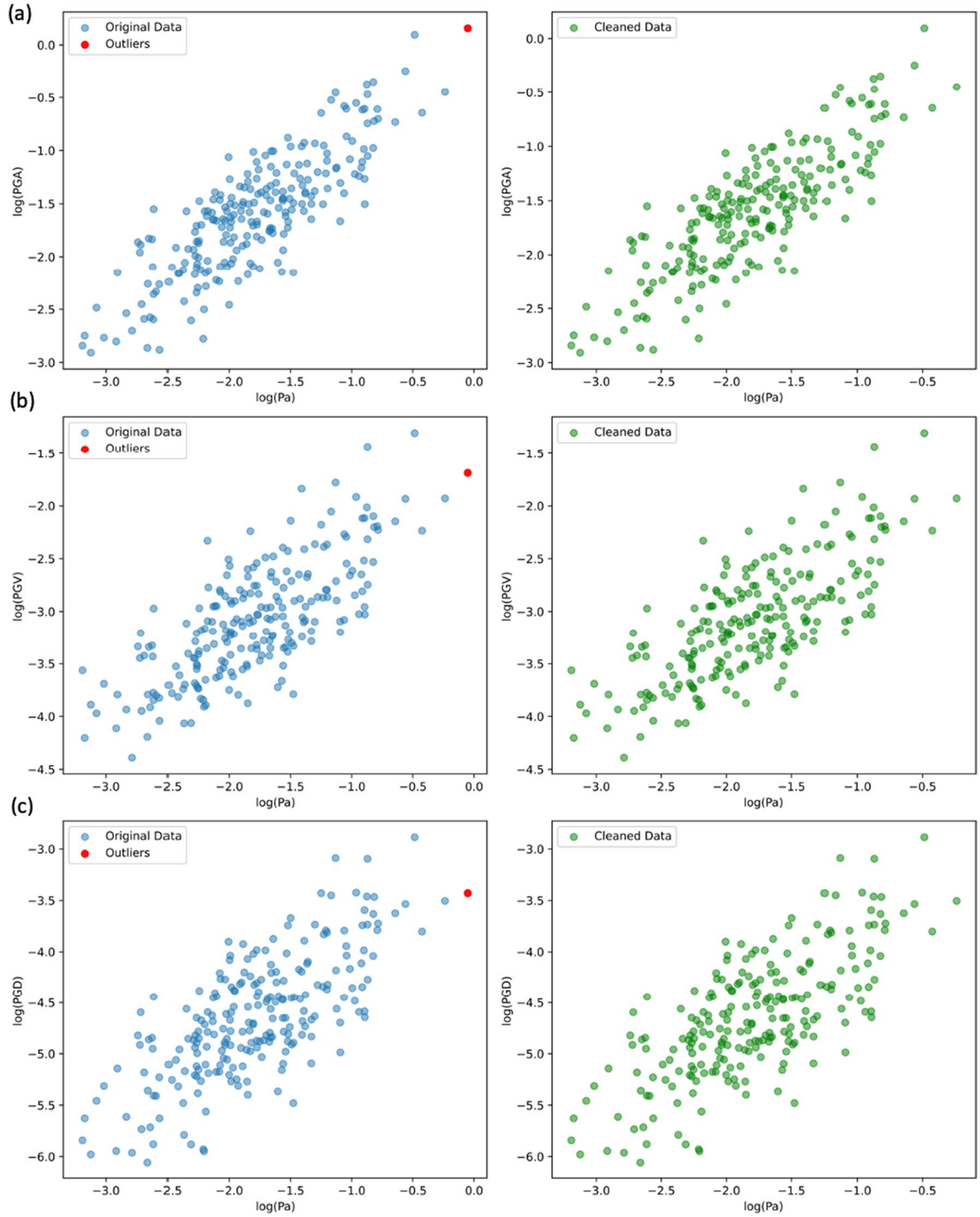

Fig. 10 It shows the original and cleaned testing data for relationships using Pa as the input parameter. Panel (**a**) displays Pa vs. PGA, panel (**b**) shows Pa vs. PGV, and panel (**c**) depicts Pa vs. PGD, with each panel comparing original data (left) and data post-outlier removal (right)

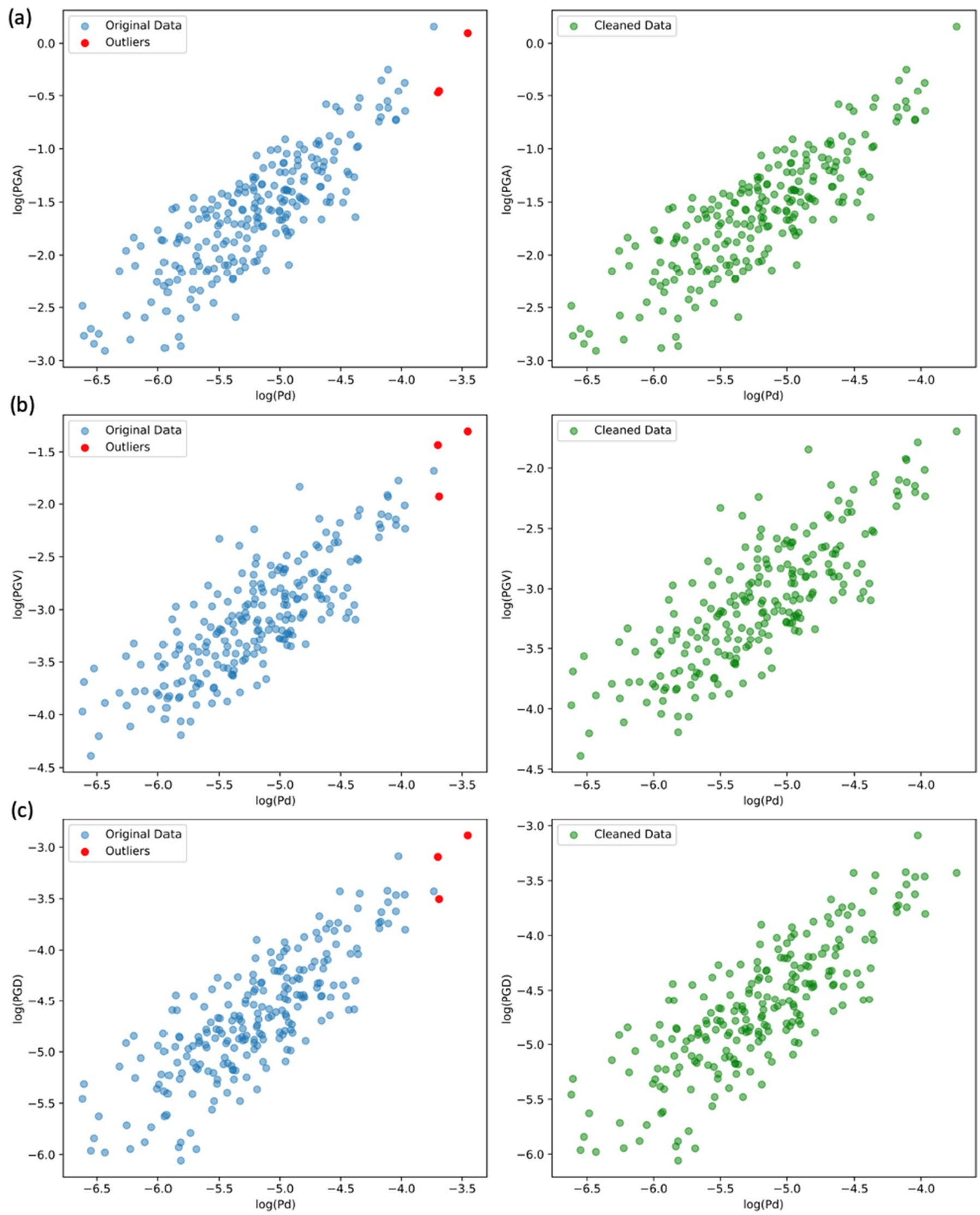

Fig. 11 It shows the original and cleaned testing data for relationships using Pv as the input parameter. Panel (**a**) displays Pv vs. PGA, panel (**b**) shows Pv vs. PGV, and panel (**c**) depicts Pv vs. PGD, with each panel comparing original data (left) and data post-outlier removal (right)

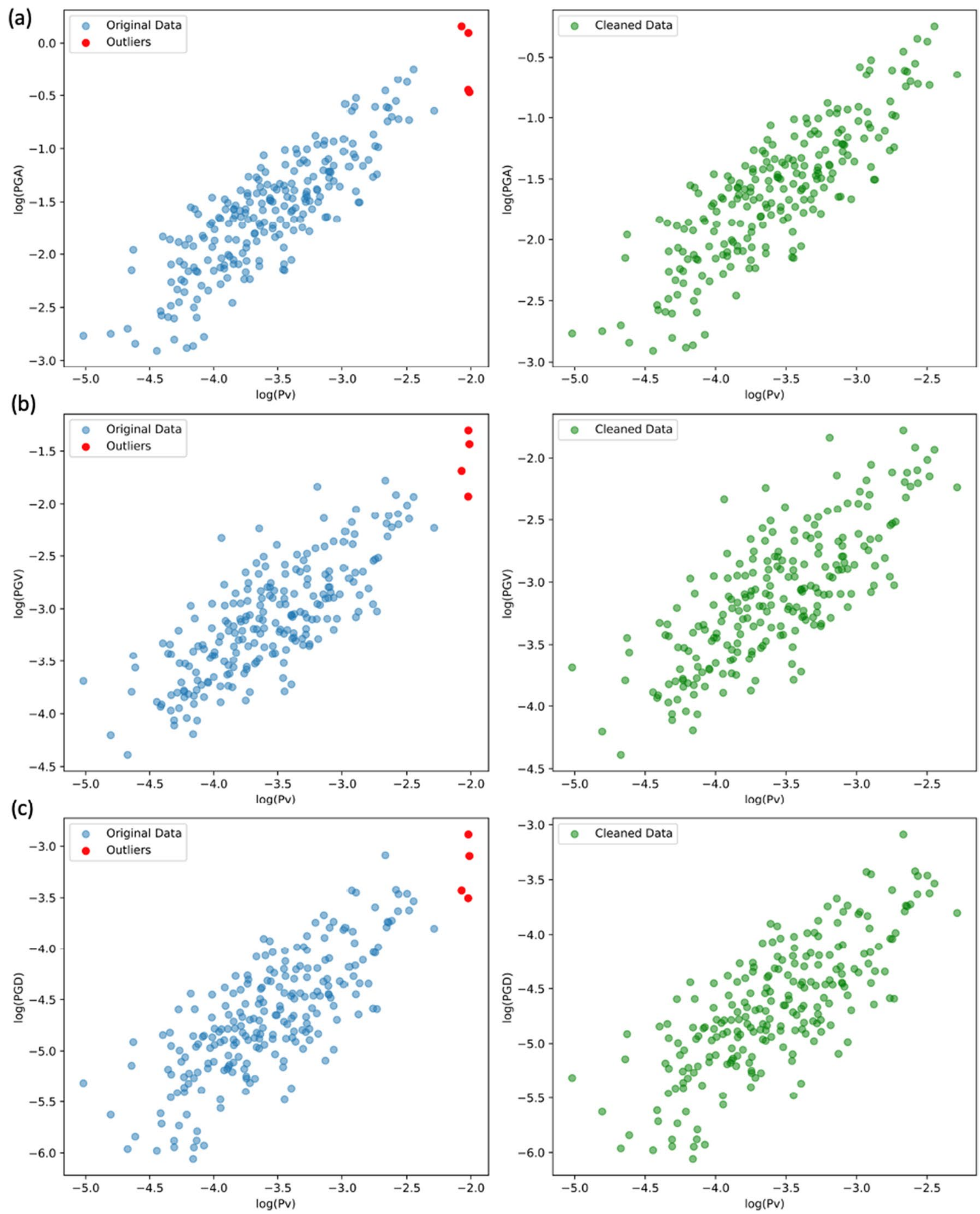

Fig. 12 It shows the original and cleaned testing data for relationships using Pv as the input parameter. Panel (**a**) displays Pv vs. PGA, panel (**b**) shows Pv vs. PGV, and panel (**c**) depicts Pv vs. PGD, with each panel comparing original data (left) and data post-outlier removal (right)

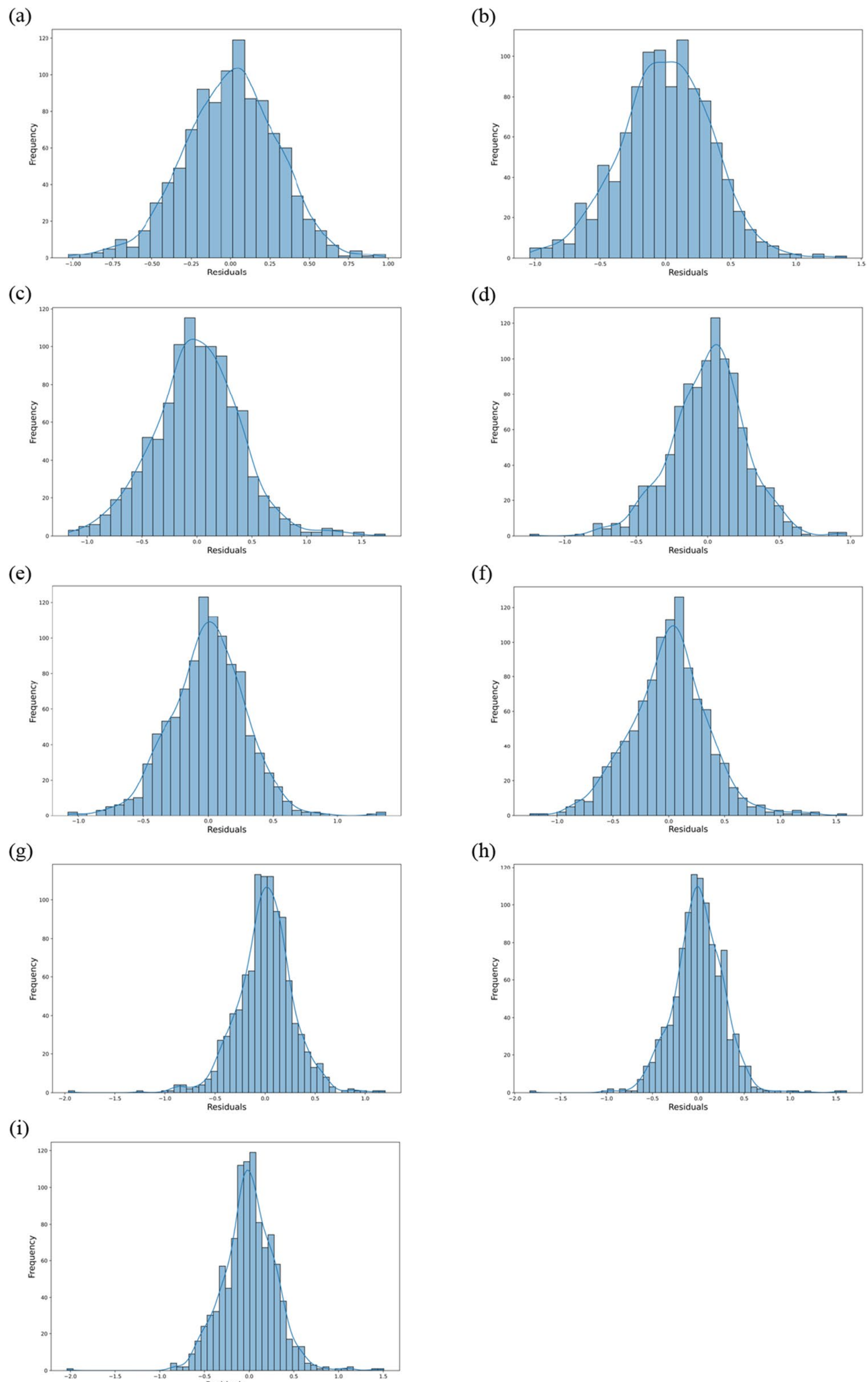

Fig. 13 it shows the histograms that show the frequency distribution of residuals in estimating S-wave amplitudes where plot (**a**) shows the histogram for Pa vs. PGA, (**b**) Pa vs. PGV, (**c**) Pa vs. PGD, (**d**) Pv vs. PGA, (**e**) Pv vs. PGV, (**f**) Pv vs. PGD, (**g**) Pd vs. PGA, (**h**) Pd vs. PGV and (**i**) Pd vs. PGD

Acknowledgements We acknowledge the New Zealand GeoNet programme and its sponsors EQC, GNS Science, LINZ, NEMA and MBIE for providing data/images used in this study.

Author contributions Conceptualisation: Chanthujan Chandrakumar; Methodology: Chanthujan Chandrakumar, Marion Lara Tan, Raj Prasanna; Software: Chanthujan Chandrakumar; Formal Analysis: Chanthujan Chandrakumar; Investigation: Chanthujan Chandrakumar; Writing—Original Draft Preparation: Chanthujan Chandrakumar; Writing—Review and Editing: Chanthujan Chandrakumar, Marion Lara Tan, Caroline Holden, Max T. Stephens, Raj Prasanna; Visualisation: Chanthujan Chandrakumar; Project Administration: Raj Prasanna, Max T. Stephens, Marion Lara Tan, Caroline Holden, Amal Punchihewa; Funding Acquisition: Raj Prasanna, Max T. Stephens, Marion Lara Tan. All authors have read and agreed to the published version of the manuscript.

Funding Open Access funding enabled and organized by CAUL and its Member Institutions. This research is funded by the Resilience to Nature's Challenges-Urban Theme 2020, QuakeCoRE - IP4: Harnessing Disruptive Technologies for Seismic Resilience, and Toka Tū Ake EQC – New Zealand.

Data availability The data supporting this study's findings are available on request from the corresponding author. Requests for access to the data can be made to Chanthujan Chandrakumar, the corresponding author of this study, at c.chandrakumar2@massey.ac.nz.

Declarations

Competing interests The authors declare no competing interests.

References

Abdalzaher MS, Soliman MS, El-Hady SM (2023) Seismic intensity estimation for earthquake early warning using optimized machine learning model. IEEE Trans Geosci Remote Sens 61. https://doi.org/10.1109/TGRS.2023.3296520

Allen RM, Kanamori H (2003) The potential for earthquake early warning in Southern California. Science 300(5620):786–789. https://doi.org/10.1126/science.1080912

Anderson H, Webb T (1994) New Zealand seismicity: patterns revealed by the upgraded National Seismograph Network. NZ J Geol Geophys 37(4). https://doi.org/10.1080/00288306.1994.9514633

Avery HR, Berrill JB, Coursey PF, Deam BL, Dewe MB, François CC, Pettinga JR, Yetton MD (2004) The Canterbury university strong-motion recording project. 13th World Conference on Earthquake Engineering, 1335

Barbur VA, Montgomery DC, Peck EA (1994) Introduction to linear regression analysis. The Statistician 43(2). https://doi.org/10.2307/2348362

Becker JS, Potter SH, Prasanna R, Tan ML, Payne BA, Holden C, Horspool N, Smith R, Johnston DM (2020) Scoping the potential for earthquake early warning in Aotearoa New Zealand: a sectoral analysis of perceived benefits and challenges. Int J Disaster Risk Reduct 51. https://doi.org/10.1016/j.ijdrr.2020.101765

Berrill J, Avery H, Dewe M, Chanerley A, Alexander NN, Dyer C, Holden C, Fry B (2011) The Canterbury Accelerograph Network (CanNet) and some results from the September 2010, M7.1 Darfield Earthquake

Boore DM (2010) Orientation-independent, nongeometric-mean measures of seismic intensity from two horizontal components of motion. Bull Seismol Soc Am. https://doi.org/10.1785/0120090400

Böse M, Hauksson E, Solanki K, Kanamori H, Wu YM, Heaton TH (2009) A new trigger criterion for improved real-time performance of onsite earthquake early warning in Southern California. Bull Seismol Soc Am 99(2 A). https://doi.org/10.1785/0120080034

Böse M, Hauksson E, Solanki K, Kanamori H, Heaton TH (2009a) Real-time testing of the on-site warning algorithm in southern California and its performance during the July 29 2008 Mw5.4 Chino Hills earthquake. Geophys Res Lett 36(5). https://doi.org/10.1029/2008GL036366

Brooks BA, Protti M, Ericksen T, Bunn J, Vega F, Cochran ES, Duncan C, Avery J, Minson SE, Chaves E (2021) Robust earthquake early warning at a fraction of the cost: ASTUTI Costa Rica. AGU Adv 2(3):e2021AV000407

Caruso A, Colombelli S, Elia L, Picozzi M, Zollo A (2017) An on-site alert level early warning system for Italy. J Geophys Res: Solid Earth 122(3). https://doi.org/10.1002/2016JB013403

Chandrakumar C, Tan ML, Holden C, Stephens MT, Prasanna R (2023) Performance analysis of P-wave detection algorithms for a community-engaged earthquake early warning system–a case study of the 2022 M5.8 Cook Strait earthquake. NZ J Geol Geophys. https://doi.org/10.1080/00288306.2023.2284276

Claerbout JF (1964) Detection of P-waves from weak sources at great distances. Geophysics 29(2):197–211. https://doi.org/10.1190/1.1439350

Clayton RW, Heaton T, Kohler M, Chandy M, Guy R, Bunn J (2015) Community seismic network: a dense array to sense earthquake strong motion. Seismol Res Lett 86(5):1354–1363. https://doi.org/10.1785/0220150094

Colombelli S, Caruso A, Zollo A, Festa G, Kanamori H (2015) A P wave-based, on-site method for earthquake early warning. Geophys Res Lett 42(5). https://doi.org/10.1002/2014GL063002

Dobry R, Borcherdt RD, Crouse CB, Idriss IM, Joyner WB, Martin GR, Power MS, Rinne EE, Seed RB (2000) New site coefficients and site classification system used in recent building seismic code provisions. Earthq Spectra 16(1). https://doi.org/10.1193/1.1586082

Dowrick DJ (1996) The modified mercalli earthquake intensity scale-revisions arising from recent studies of New Zealand earthquakes. Bull New Z Natl Soc Earthq Eng, 29(2):92–102

Dowrick DJ, Hancox GT, Perrin ND, Dellow GD (2008) The modified mercalli intensity scale - revisions arising from New Zealand experience. Bull New Z Soc Earthq Eng 41(3). https://doi.org/10.5459/bnzsee.41.3.193-205

Draper NR, Smith H (2014) Applied regression analysis. In: Applied regression analysis. https://doi.org/10.1002/9781118625590

GeoNet (2017) GeoNet Home. https://www.geonet.org.nz/. Accessed 26 Apr 2024

GeoNet (2023) GeoNet statistics. https://www.geonet.org.nz/earthquake/statistics_long. Accessed 9 Jun 2023

Gianluca Malato (2021) Outlier identification using Interquartile Range. Towards Data Science. https://towardsdatascience.com/

outlier-identification-using-interquartile-range-74f5de12932a. Accessed 26 Apr 2024
GNS Science (2023) Earthquake early warning in New Zealand. GNS Science. https://www.gns.cri.nz/news/earthquake-early-warning-in-new-zealand/. Accessed 30 Apr 2024
Griffith A, Headley JD (1997) Using a weighted score model as an aid to selecting procurement methods for small building works. Constr Manage Econ 15(4):341–348. https://doi.org/10.1080/014461997372890
Holland A (2003) Earthquake data recorded by the MEMS accelerometer: field testing in Idaho. Seismol Res Lett 74(1). https://doi.org/10.1785/gssrl.74.1.20
Hoshiba M, Iwakiri K, Hayashimoto N, Shimoyama T, Hirano K, Yamada Y, Ishigaki Y, Kikuta H (2011) Outline of the 2011 off the pacific coast of tohoku earthquake (M w 9.0) -earthquake early warning and observed seismic intensity. Earth Planets and Space 63(7):547–551. https://doi.org/10.5047/eps.2011.05.031
Hsu T-Y, Huang C-W (2021) Onsite early prediction of PGA using CNN with multi-scale and multi-domain P-Waves as input. Front Earth Sci 9. https://doi.org/10.3389/feart.2021.626908
Jon Reilly (2024) Overfitting and underfitting in machine learning. https://www.akkio.com/post/overfitting-and-underfitting-in-machine-learning. Accessed 23 Apr 2024
Kanamori H (2005) Real-time seismology and earthquake damage mitigation. Annu Rev Earth Planet Sci. https://doi.org/10.1146/annurev.earth.33.092203.122626
Kodera Y (2018) Real-time detection of rupture development: earthquake early warning using P waves from growing ruptures. Geophys Res Lett 45(1):156–165. https://doi.org/10.1002/2017GL076118
Lyu Y, Li H, Sayagh M, Jiang ZM, Hassan AE (2021) An empirical study of the impact of data splitting decisions on the performance of AIOps solutions. ACM Trans Softw Eng Methodol 30(4). https://doi.org/10.1145/3447876
Moratalla JM, Goded T, Rhoades DA, Canessa S, Gerstenberger MC (2020) New ground motion to intensity conversion equations (GMICEs) for New Zealand. Seismol Res Lett 92(1). https://doi.org/10.1785/0220200156
Nakamura Y (2004) UrEDAS, urgent earthquake detection and alarm system, now and future. 13th World Conference on Earthquake Engineering, 908
Nicholas Morpus (2024) A step-by-step guide for using a weighted scoring model. The Ascent
Olson EL, Allen RM (2005) The deterministic nature of earthquake rupture. Nature 438(7065):212–215. https://doi.org/10.1038/nature04214
Peng C, Jiang P, Chen Q, Ma Q, Yang J (2019) Performance evaluation of a dense MEMS-based seismic sensor array deployed in the Sichuan-Yunnan border region for earthquake early warning. Micromachines 10(11). https://doi.org/10.3390/mi10110735
Potter SH, Becker JS, Johnston DM, Rossiter KP (2015) An overview of the impacts of the 2010–2011 Canterbury earthquakes. Int J Disaster Risk Reduct 14. https://doi.org/10.1016/j.ijdrr.2015.01.014
Pragati Baheti (2021) What is overfitting in deep learning [+10 ways to avoid it]. https://www.v7labs.com/blog/overfitting. Accessed 23 Apr 2024
Prasanna R, Chandrakumar C, Nandana R, Holden C, Punchihewa A, Becker JS, Jeong S, Liyanage N, Ravishan D, Sampath R, Tan ML (2022) Saving precious seconds—A novel approach to implementing a low-cost earthquake early warning system with node-level detection and alert generation. Informatics 9(1):25. https://doi.org/10.3390/informatics9010025
Rydelek P, Horiuchi S (2006) Earth science: is earthquake rupture deterministic? Nature 442(7100). https://doi.org/10.1038/nature04963
Shearer PM (2009) Introduction to seismology, 2nd edn, vol 4, issue 3. Cambridge University Press, pp 20–25
Stevenson JR, Kachali H, Whitman Z, Seville E, Vargo J, Wilson T (2011) Preliminary observations of the impacts the 22 February Christchurch earthquake had on organisations and the economy: a report from the field (22 February – 22 March 2011). Bull New Z Soc Earthq Eng 44(2). https://doi.org/10.5459/bnzsee.44.2.65-76
Stevenson JR, Becker J, Cradock-Henry N, Johal S, Johnston D, Orchiston C, Seville E (2017) Economic and social reconnaissance: Kaikōura earthquake 2016. Bull New Z Soc Earthq Eng 50(2). https://doi.org/10.5459/bnzsee.50.2.343-351
Taylor CK (2018) What is the interquartile range rule? https://www.thoughtco.com/what-is-the-interquartile-range-rule-3126244. Accessed 26 Apr 2024
Tigran P (2022) Overfitting and underfitting in machine learning. SuperAnnotate. https://www.superannotate.com/blog/overfitting-and-underfitting-in-machine-learning. Accessed 30 Apr 2024
Tsuno S (2021) Applicability of on-site P-Wave earthquake early warning to seismic data observed during the 2011 off the Pacific Coast of Tohoku Earthquake, Japan. Front Earth Sci 9. https://doi.org/10.3389/feart.2021.681199
Virtanen P, Gommers R, Oliphant TE, Haberland M, Reddy T, Cournapeau D, Burovski E, Peterson P, Weckesser W, Bright J, van der Walt SJ, Brett M, Wilson J, Millman KJ, Mayorov N, Nelson ARJ, Jones E, Kern R, Larson E, … Vázquez-Baeza Y (2020) SciPy 1.0: fundamental algorithms for scientific computing in Python. Nat Methods 17(3). https://doi.org/10.1038/s41592-019-0686-2
Wang Y, Li S, Song J (2020) Threshold-based evolutionary magnitude estimation for an earthquake early warning system in the Sichuan–Yunnan region, China. Sci Rep 10(1):1–12. https://doi.org/10.1038/s41598-020-78046-2
Wells DL, Coppersmith KJ (1994) New empirical relationships among magnitude, rupture length, rupture width, rupture area, and surface displacement. Bull-Seismol Soc Am 84(4):974–1002. https://doi.org/10.1785/bssa0840040974
Will Koehrsen (2018) Overfitting vs. Underfitting: A complete example. Towards Data Science. https://towardsdatascience.com/overfitting-vs-underfitting-a-complete-example-d05dd7e19765. Accessed 30 Apr 2024
Wu Y-M (2019) Performance of a low-cost earthquake early warning System (P-Alert) and shake map production during the 2018 mw 6.4 Hualien (Taiwan) Earthquake. Geophys Res Abstracts 21:1
Wu YM, Kanamori H (2005a) Experiment on an onsite early warning method for the Taiwan early warning system. Bull Seismol Soc Am 95(1):347–353. https://doi.org/10.1785/0120040097
Wu YM, Kanamori H (2005b) Rapid assessment of damage potential of earthquakes in Taiwan from the beginning of P waves. Bull Seismol Soc Am 95(3):1181–1185. https://doi.org/10.1785/0120040193
Wu Y-M, Kanamori H (2008) Development of an earthquake early warning system using real-time strong motion signals. Sensors 8(1):1–9. https://doi.org/10.3390/s8010001
Wu Y-M, Mittal H (2021) A review on the development of earthquake warning system using low-cost sensors in Taiwan. Sensors 21(22). https://doi.org/10.3390/s21227649
Wu YM, Zhao L (2006) Magnitude estimation using the first three seconds P-wave amplitude in earthquake early warning. Geophys Res Lett 33(16):4–7. https://doi.org/10.1029/2006GL026871
Wu YM, Chen DY, Lin TL, Hsieh CY, Chin TL, Chang WY, Li W, Sen, Ker SH (2013) A high-density seismic network for earthquake early warning in Taiwan based on low cost sensors. Seismol Res Lett 84(6):1048–1054. https://doi.org/10.1785/0220130085
Yamamoto S, Rydelek P, Horiuchi S, Wu C, Nakamura H (2008) On the estimation of seismic intensity in earthquake early warning systems. Geophys Res Lett 35(7). https://doi.org/10.1029/2007GL033034
Zhang H, Thurber C, Rowe C (2003) Automatic P-wave arrival detection and picking with multiscale wavelet analysis for

single-component recordings. Bull Seismol Soc Am 93(5):1904–1912. https://doi.org/10.1785/0120020241

Zhu J, Li S, Song J (2022) Hybrid deep-learning network for rapid on-site peak ground velocity prediction. IEEE Trans Geosci Remote Sens 60. https://doi.org/10.1109/TGRS.2022.3230829

Zollo A, Lancieri M, Nielsen S (2006) Earthquake magnitude estimation from peak amplitudes of very early seismic signals on strong motion records. Geophys Res Lett 33(23):2–7. https://doi.org/10.1029/2006GL027795

Zollo A, Amoroso O, Lancieri M, Wu YM, Kanamori H (2010) A threshold-based earthquake early warning using dense accelerometer networks. Geophys J Int 183(2). https://doi.org/10.1111/j.1365-246X.2010.04765.x

Zollo A, Colombelli S, Elia L, Emolo A, Festa G, Iannaccone G, Martino C, Gasparini P (2014) An integrated regional and on-site earthquake early warning system for Southern Italy: Concepts, methodologies and performances. March, pp 117–137. https://doi.org/10.1007/978-3-642-12233-0_7